

ORIGINAL ARTICLE

Hyperactive MEK1 Signaling in Cortical GABAergic Neurons Promotes Embryonic Parvalbumin Neuron Loss and Defects in Behavioral Inhibition

Michael C. Holter¹, Lauren T. Hewitt^{1,6}, Kenji J. Nishimura^{1,6}, Sara J. Knowles¹, George R. Bjorklund¹, Shiv Shah¹, Noah R. Fry¹, Katherina P. Rees¹, Tanya A. Gupta², Carter W. Daniels^{2,7}, Guohui Li³, Steven Marsh⁴, David Michael Treiman⁴, Michael Foster Olive², Trent R. Anderson³, Federico Sanabria², William D. Snider⁵ and Jason M. Newbern¹

¹School of Life Sciences, Arizona State University, Tempe, AZ 85287, USA, ²Department of Psychology, Arizona State University, Tempe, AZ 85287, USA, ³College of Medicine, University of Arizona, Phoenix, AZ 85004, USA, ⁴Barrow Neurological Institute, Phoenix, AZ 85013, USA, ⁵University of North Carolina Neuroscience Center, The University of North Carolina School of Medicine, Chapel Hill, NC 27599, USA, ⁶Current address: Interdepartmental Neuroscience Graduate Program, University of Texas, Austin, TX 78712, USA and ⁷Current address: Department of Psychiatry, Columbia University, New York, NY 10032, USA

Address correspondence to Jason M. Newbern, School of Life Sciences, Arizona State University, PO Box 84501, Tempe, AZ 85287-4501, USA.
Email: jason.newbern@asu.edu.

Abstract

Many developmental syndromes have been linked to genetic mutations that cause abnormal ERK/MAPK activity; however, the neuropathological effects of hyperactive signaling are not fully understood. Here, we examined whether hyperactivation of MEK1 modifies the development of GABAergic cortical interneurons (CINs), a heterogeneous population of inhibitory neurons necessary for cortical function. We show that GABAergic-neuron specific MEK1 hyperactivation in vivo leads to increased cleaved caspase-3 labeling in a subpopulation of immature neurons in the embryonic subpallial mantle zone. Adult mutants displayed a significant loss of parvalbumin (PV), but not somatostatin, expressing CINs and a reduction in perisomatic inhibitory synapses on excitatory neurons. Surviving mutant PV-CINs maintained a typical fast-spiking phenotype but showed signs of decreased intrinsic excitability that coincided with an increased risk of seizure-like phenotypes. In contrast to other mouse models of PV-CIN loss, we discovered a robust increase in the accumulation of perineuronal nets, an extracellular structure thought to restrict plasticity. Indeed, we found that mutants exhibited a significant impairment in the acquisition of behavioral response inhibition capacity. Overall, our data suggest PV-CIN development is particularly sensitive to hyperactive MEK1 signaling, which may underlie certain neurological deficits frequently observed in ERK/MAPK-linked syndromes.

Key words: ADHD, development, ERK1/2, ganglionic eminence, RASopathy

Introduction

The RAS/RAF/MEK/ERK (ERK/MAPK or ERK1/2) pathway is a well-known intracellular signaling cascade that is dynamically regulated during development (Samuels et al. 2009; Roskoski 2012). Mutations in RAF/MEK/ERK or upstream regulators, such as *PTPN11*/*SHP2*, *NF1*, or *SYNGAP1*, are the cause of a family of syndromes known collectively as the RASopathies. These syndromes usually exhibit hyperactive ERK/MAPK signaling and are commonly associated with intellectual disability, developmental delay, attention deficit hyperactivity disorder (ADHD), autism, and epilepsy (Tidyman and Rauhen 2016). *MAPK3/ERK1* is also present in a frequently mutated region of 16p11.2 linked to autism spectrum disorder (ASD), and animal models of certain ASDs exhibit altered ERK/MAPK activity (Vorstman et al. 2006; Kumar et al. 2008; Osterweil et al. 2010; Pucilowska et al. 2018). Therapeutic approaches for these disorders are limited, due in part to an incomplete understanding of the cell-specific effects of pathological ERK/MAPK signaling on brain development.

Delineating the precise consequences of aberrant ERK/MAPK pathway activation on specific cellular subtypes will provide important insight into normal cortical development and possibly certain neurodevelopmental disorders. Coordinated interactions between multiple neuronal subtypes are essential for normal brain function. In the developing cerebral cortex, ERK/MAPK signaling is necessary for the specification, outgrowth, and functional characteristics of certain glutamatergic projection neurons (PNs) and glia derived from the dorsal ventricular zone (Clement et al. 2012; Li et al. 2012; Ishii et al. 2013; Ehrman et al. 2014; Ozkan et al. 2014; Aoidi et al. 2018). We have previously shown that ERK/MAPK inactivation, specifically in developing cortical PNs, leads to reduced inhibitory input (Xing et al. 2016). Indeed, GABAergic cortical interneurons (CINs) are essential for the maturation and function of neural circuits and are disrupted in models of fragile X and Rett syndromes (Chao et al. 2010; Paluszkiwicz et al. 2011). Yet, the role of ERK/MAPK signaling in the development of this critical neuronal population is less clear. Moreover, when compared with PNs, it is unknown whether ERK/MAPK activation has similar or distinct effects on CIN specification and maturation.

Locally projecting parvalbumin (PV)- and somatostatin-expressing (SST) CINs are generated in the embryonic medial ganglionic eminence (MGE) and migrate tangentially into the cortex (Tamamaki et al. 1997; Lavdas et al. 1999; Marin and Rubenstein 2003; Wonders and Anderson 2006; Gelman and Marín 2010). The transcriptional machinery necessary for CIN specification and maturation has been well-studied (Paul et al. 2017; Lim et al. 2018; Mayer et al. 2018; Mi et al. 2018). CIN development is also regulated by a range of extrinsic trophic signals, such as BDNF/TRKB, GDNF/GFR α 1, HGF/MET, and NRG/ERBB4 (Flames et al. 2004; Pozas and Ibanez 2005; Bae et al. 2010; Fazzari et al. 2010; Perrinjaquet et al. 2011). These factors activate core receptor tyrosine kinase (RTK)-linked intracellular signaling components, such as Ras, PI3K/Akt, PLC, and ERK/MAPK. Upstream RASopathy-associated mutations in neurofibromin 1 (*NF1*) and *Syngap1* enhance Ras activity; increase downstream signaling via PI3K/Akt, ERK/MAPK, and other cascades; and have been shown to impair CIN specification and/or inhibitory circuit function (Cui et al. 2008; Brown et al. 2012; Anastasakis and Gutmann 2014; Berryer et al. 2016; Angara et al. 2020). Since the PI3K/Akt-associated factors PTEN, PDK1, and TSC1 are known to regulate CIN survival and specification, the CIN-autonomous effects of downstream pathological RAF/MEK/ERK activation on GABAergic circuit

development and cortical function in RASopathies are less clear (Vogt et al. 2015; Malik et al. 2019; Wei et al. 2020).

Here, we sought to selectively manipulate downstream ERK/MAPK signaling by hyperactivating MEK1 specifically in mouse embryonic GABAergic CINs *in vivo*. We show that Cre-dependent expression of constitutively active MEK1^{S217/221E} (*caMEK1*) in CINs with two different Cre lines, *Slc32a1:Cre* and *Nkx2.1:Cre*, leads to caspase-3 activation in a subset of embryonic GABAergic neurons and reduced CIN number by late embryogenesis. Even though *caMEK1* is expressed in multiple CIN subclasses, we noted a significant reduction in the number of mature PV-CINs, but not SST-CINs, which coincided with an increased risk of mild seizure-like activity. In contrast with past models of genetic syndromes exhibiting PV-CIN loss, we found a surprising increase in the extent of perineuronal net (PNN) accumulation around these cells (Steullet et al. 2017). PNNs are well known for their role in regulating developmental critical periods and typically reduce neural plasticity in adulthood. We found that *caMEK1* mutants exhibited normal locomotor, anxiety-like, and social behaviors, but deficits in the acquisition of a behavioral response inhibition task. Our findings indicate that MEK1 hyperactivation is sufficient to drive select GABAergic-neuron autonomous defects in CIN maturation and cognitive phenotypes associated with neurodevelopmental syndromes. These data suggest deficits in PV-CIN survival or function may be a candidate neuropathological mechanism in ERK/MAPK-linked genetic disorders.

Materials and Methods

Mice

All transgenic mice were handled and housed in accordance with the guidelines of the Institutional Animal Care and Use Committee at Arizona State University, the University of Arizona, and Barrow Neurological Institute, kept on a daily 12-h light-dark cycle, and fed *ad libitum*. *Slc32a1:Cre* (JAX Stock #028862; Vong et al. 2011), *Nkx2.1:Cre* (JAX Stock #008661; Xu et al. 2008), or *Dlx5/6:Cre* (JAX Stock #008119; Monory et al. 2006) mice were crossed with *CAG-lox-STOP-lox-Mek1*^{S217/221E} (*caMek1*) mice on a mixed genetic background to generate double heterozygous mutants expressing *caMek1* in Cre-expressing cell types. *CaMek1* mice were kindly provided by Dr Maïke Krenz and Dr Jeffrey Robbins (Krenz et al. 2008). Littermates expressing Cre recombinase were utilized as controls unless otherwise indicated. Cre-dependent tdTomato (Ai9) or EYFP (Ai3) strains were used to endogenously label Cre-expressing cells. Genomic DNA was extracted from tail or toe samples for standard genotyping by PCR using the following primer combinations: (listed 5'-3'): Cre—TTGCAAGAACCTGATGGAC and CATTGCTGCTCACTTGGTCTG to amplify a 266-bp fragment; *caMek1*^{S217/221E}—GTACCAGCTCGGCGGAGACCAA and TTGATCACAGCAATGCTAACTTTC to amplify a 600-bp fragment; Ai3/Ai9—AAGGGAGCTGCAGTGGAGTA, CCGAAAATCTGTGGGAAGTC, ACATGGTCTGCTGGAGTTC, and GGCATTAAAGCAGCGTATCC to amplify a 297 bp wt *Rosa26* segment and a 212 bp Ai3/Ai9 allele.

Tissue Preparation and Immunostaining

Mice of the appropriate postnatal age were fully anesthetized and transcardially perfused with PBS followed by cold 4% PFA in PBS. Brains were then dissected, postfixed at 4 °C, and sectioned with a vibratome or cryopreserved in 30% sucrose and OCT. For embryonic brains, timed-bred embryos were collected at the

appropriate embryonic age, immersion fixed in cold 4% PFA in PBS, incubated in serial sucrose concentrations in PBS, and cryopreserved. Free floating or slide-mounted sections were rinsed in PBS and blocked in a buffer containing 0.05–0.2% Triton 5% normal donkey serum (NDS) in PBS before incubating in primary antibody solution. Sections were then rinsed and incubated in secondary antibody solutions containing Alexa-Fluor 488, 568, or 647 conjugated antirabbit, antigoat, or antichick antibodies diluted in blocking solution. Tissue was rinsed in PBS and cover-slipped for microscopic analysis. Streptavidin-conjugated fluorophores were used to visualize WFA labeling.

Microscopy and Image Analysis

Images were collected on a Zeiss (LSM710 or LSM800) laser scanning confocal microscope and optimized for brightness and contrast in Adobe Photoshop. Confocal images of at least three anatomically matched sections that include a brain region of interest were quantified for labeled cell density by observers blinded to genotype. For estimating labeled cell density in the cortex, a column spanning all cortical layers was defined, the cross-sectional area was measured, and the number of labeled cells was assessed. The proportion of cells colabeled with Cre-dependent fluorescent reporters was also determined for select experiments. Quantification of cellular labeling was averaged across all images collected from an individual mouse. At least three mice were collected for each genotype and results were analyzed using Student's *t*-tests unless indicated otherwise.

We quantified the extent of inhibitory synapse labeling in the perisomal domain of excitatory neurons from confocal images of VGAT/NEUN/GFP colabeled sections. Confocal images were collected using optimal Airyscan settings for a 63× 1.4 NA objective on a Zeiss LSM800 with the same acquisition parameters, laser power, gain, and offset for VGAT detection. NEUN⁺/GFP⁻ neurons in S1 layer 2/3 with a pyramidal morphology and residing 5–10 μm from the tissue section surface were randomly selected by a blinded observer. NEUN⁺ soma were outlined in Photoshop and a ring 1.8 μm in thickness was then established to specify the perisomatic space. VGAT immunolabeling from perisomatic regions of interest were imported into ImageJ where the autothreshold algorithm, “Moments,” was utilized to define the total area of perisomatic VGAT labeling in an unbiased manner. The perisomatic VGAT-labeled area was then normalized to the total perisomatic area for that neuron. A total of 48 control and 53 mutant neurons from 3 different mice were analyzed. A similar approach was utilized to quantify VGAT labeling in areas enriched in dendrites by analyzing randomly selected regions of the layer 2/3 neuropil that did not contain NEUN-labeled somas.

EEG Recordings and Seizure Threshold Assessment

Adult *caMek1*, *Slc32A1:Cre* mutant and *Slc32A1:Cre* control mice were assessed for epileptiform activity with bilateral 175-μm tungsten wires implanted in the forebrain. After recovery from electrode implantation, mice were connected to suspended EEG leads, housed individually, and monitored daily in home cages for seizure-like activity using a 128 channel Natus Medical EEG machine. EEG recordings were examined for synchronous firing between hemispheres, and representative epileptiform traces were acquired. Following intracranial recording, mice were injected with the seizure-inducing compound, pentylenetetrazol (PTZ; Sigma P6500). Mice were gently restrained and the tail vein was intravenously injected with 0.34 mL/min of 5 mg/mL

PTZ in 0.9% saline 10USP heparin by automated pump. Initial onset of seizure was defined as the first sign of involuntary movement by an observer blinded to genotype. Time to seizure was recorded and PTZ μg/g of body weight was calculated.

Slice Electrophysiology

caMek1^{+/-}, *Nkx2.1:Cre^{+/-}*, *Ai9^{+/-}* mutant and *Nkx2.1:Cre^{+/-}*, *Ai9^{+/-}* control mice were sacrificed between postnatal day 21 to 23 for in vitro slice electrophysiology. Brain slicing and preparation were performed as reported previously (Nichols et al. 2018). Briefly, mice were deeply anesthetized by isoflurane inhalation, brains were quickly removed, and coronal slices (350 μm) of the somatosensory cortex were collected on a vibratome (VT 1200; Leica, Nussloch, Germany) in fully oxygenated (95% O₂, 5% CO₂), ice-cold artificial cerebral spinal fluid (aCSF) containing (in mM): 126 NaCl, 26 NaHCO₃, 2.5 KCl, 10 glucose, 1.25 Na₂H₂PO₄·H₂O, 1 MgSO₄·7H₂O, 2 CaCl₂·H₂O, pH 7.4. The slices were incubated in the same aCSF at 32 °C for 30 min before being allowed to recover at room temperature for an additional 30 min. After recovery, slices were transferred into recording chamber and perfused continuously with aCSF at 32 °C at a rate of 1–2 mL/min.

Whole-cell patch clamp recordings were performed on tdTomato-positive fast-spiking (FS) interneurons in the somatosensory cortex layer V/VI (L5/6) by using an Axon 700B amplifier. The FS neurons were identified by lack of an emerging apical dendrite and their intrinsic firing response to current injection (Anderson et al. 2010; McCormick et al. 1985). Clampex 10.6 (Molecular Devices) was used to collect data and pipettes (2–5 MΩ) were pulled from borosilicate glass (BF150-110-10, Sutter Instruments) by using a micropipette puller (Model P-1000, Sutter Instruments), filled with an internal solution that contains (in mM): 135 K-Gluconate, 4 KCl, 2 NaCl, 10 HEPES, 4 EGTA, 4 Mg ATP, and 0.3 Na Tris, calculated E_{Cl⁻} = 80 mV. The stability of the recordings was monitored during the experiments, and only the recordings with the series resistances (R_s) less than both 25 MΩ and 20% of the membrane resistances were chosen for analysis.

Electrophysiological recordings and analysis were performed as previously described (Anderson et al. 2010; Nichols et al. 2018). In brief, resting membrane potential was measured prior to induced current steps. For the input resistance calculation, the steady plateau of the voltage responding to the current input of –50 pA step with 1-s duration was used. An exponential fit to the discharging phase of voltage response to the input resistance current step was used to calculate the time constant and in turn the membrane capacitance (C_m). Firing frequency was calculated as the number of action potential spikes (Aps) elicited per current step (–150 pA to 300 pA, 50pA steps, 1 s). The frequency (F) – current (I) slope was calculated as the number of induced action potentials (APs) divided by the current step (number of APs at 150 pA – number of APs at 100pA)/(150 pA – 100 pA). Adaptation index was calculated as the ratio of the first interspike interval over the last (i.e., F_{1st ISI}/F_{last ISI}). Rheobase was measured as the minimum 50-ms long current step that induced an action potential. Action potential properties were measured following delivery of a short intracellular current pulse (0.5 ms, 1 nA). Recording of spontaneous postsynaptic currents (sPSCs) was performed under voltage clamp for 5 min at a holding potential of –70 mV. Data were analyzed using Clampfit (Pclamp 10, Molecular Devices) and Mini Analysis (Synaptosoft).

Unpaired Student's t-test and two-way ANOVA with Bonferroni post hoc tests were used for statistical analysis.

Behavioral Assessments

Open Field Test

The open field test was used to test voluntary locomotor capabilities and anxiety-like behavior. The apparatus consisted of a 40 × 40 cm arena enclosed by 30-cm-high opaque walls. A single 60 W bulb was positioned to brightly illuminate the center of the chamber with dim lighting near the walls. Mice were placed into the apparatus and recorded for a total of 10 min. Video data were analyzed for total distance traveled and time spent in the center quadrant.

Elevated Plus Maze

The elevated plus maze was constructed from black polycarbonate, elevated 81 cm off the ground, and oriented in a plus formation with two 12 × 55 cm open arms and two 12 × 55 cm closed arms extending from an open 12 × 12 cm center square. Closed arm walls were 40 cm high extending from the base of the arm at the center square. The apparatus was lit with a 60 W bulb with light concentrated on the center square. At the beginning of the trial, mice were placed in the center square, facing the south open arm, and recorded while freely exploring for 5 min.

Social Approach Assay

The social approach apparatus was made of transparent plexiglass and contained three 20 × 30 × 30 cm chambers (total dimensions 60 × 30 × 30 cm) connected by open doorways. Prior to experimental social trials, mice were habituated to the apparatus and allowed to freely explore all three chambers for 5 min. At the end of the 5 min, mice were removed and placed in their home cage. A sex- and age-matched stimulus mouse was then placed into a small empty cage in chamber 1 of the apparatus. The experimental mouse was reintroduced to the center chamber (chamber 2) of the apparatus and recorded while freely exploring for 10 min. The time spent in the chamber with the stimulus mouse (chamber 1) or the empty chamber (chamber 3) was then measured.

Fixed Minimum Interval

Twenty-four adult mice (12 *Slc32A1:Cre* mice: 5 males, 7 females; 12 *caMek1, Slc32A1:Cre* mice: 6 males, 6 females) were kept on a 12-h reverse light-dark cycle. Animals had free access to water in their home cages, but access to food was gradually reduced in the week prior to behavioral training, where 1 h of food access was provided 30 min after the end of each daily training session. Body weights were maintained such that mice lost no more than 15% of starting body weight. Behavioral testing was conducted in 8 MED Associates (St. Albans, VT, USA) modular test chambers (240 mm length × 200 mm width × 165 mm height; ENV-307W). Each chamber was enclosed in a sound- and light-attenuating cabinet (ENV-022V) equipped with a fan for ventilation that provided masking noise of approximately 60 dB (ENV-025-F28). The back wall and hinged front door of each chamber were made of plexiglass. The side walls of the chamber were made of aluminum, and the right wall contained the manipulanda and reward receptacle. The floor was composed of thin metal bars. A circular reward receptacle was positioned in the center of the front panel and equipped with a head-entry detector (ENV-302HD), a liquid dipper (ENV-302W-S), and a yellow LED (ENV-321W). The reward receptacle was flanked by a

nose-poke device including an LED illuminator (ENV-314M). The chamber was fitted with a house light (ENV-315 W) at ceiling level above the back wall (ENV-323AW) and a 4.5-kHz tone generator (ENV-323HAM). Experimental programs were arranged via a MED PC interface connected to a PC controlled by MED-PC IV software. All behavioral sessions were 30 min long, including a 3-min warm-up period during which no stimuli were activated.

Reinforcement Training and Autoshaping

Mice were first trained to obtain 0.1 cc of diluted sweetened condensed milk from the liquid dipper (the reinforcer) in the reward receptacle. Following the 3-min warm-up period, a reinforcer was made available, followed by consistent reinforcer delivery at variable, pseudorandomly selected intertrial intervals (ITIs) for the remainder of the session (mean = 45 s). No stimuli were activated during ITIs. When the dipper was activated and a reinforcer was available, a 2.9-kHz tone, the head-entry LED, and the house light were turned on. The reinforcer remained available until it was obtained by the mouse, which deactivated the 2.9-kHz tone, the LED, and the house light. The dipper remains activated for 2.5 s after the mouse obtains the reinforcer. Following 5 sessions of reinforcement training, the procedure was modified for 5 autoshaping sessions, for which, in the last 8 s of each ITI, the LED inside of the nose-poke device was turned on. The nose-poke LED was then turned off and reinforcement was delivered as described. If the mouse nose-poked the device during the time when the LED was on, it was turned off and reinforcement was delivered immediately. The autoshaping procedure was then modified for another 5 sessions such that reinforcement delivery was contingent upon a single nose-poke to the nose-poke device when its LED was illuminated and the ITI was reduced to 10 s.

Fixed Minimum Interval Training

Mice were then trained on the fixed minimum interval (FMI) schedule. After the 3-min warm-up period, the house light was deactivated. A nose-poke ("initiating response") activated the nose-poke LED and marked the beginning of the interresponse time (IRT). A subsequent head entry into the reward receptacle ("terminating response") terminated the IRT. Reinforcement was delivered only if the IRT was longer than the criterion time, which was dependent upon the FMI schedule. IRTs shorter than the criterion time terminated without reinforcement and deactivated the nose-poke LED, and another trial could be immediately initiated. IRTs greater than or equal to the criterion time resulted in delivery of reward, deactivation of the nose-poke LED, a 2.5-s duration 2.9-kHz tone, and subsequent removal of the liquid dipper. House lights were then activated for a 10-s ITI, after which house light deactivation indicated a new trial could be initiated via nose-poke. The time between the end of the ITI and the nose-poke initiating response was measured and termed the "latency to initiate" (LTI). All mice were initially trained on an FMI schedule with a criterion time of 0.5 s (FMI 0.5 s) until stability was achieved. The FMI 0.5-s condition was implemented to acclimate mice to the task and is not used to evaluate response inhibition capacity. Performance was considered stable when a nonsignificant linear regression for mean median IRTs across 5 consecutive sessions was achieved, using a significance criterion of 0.05. Following stability on the FMI 0.5-s schedule, subjects experience FMI 2, 4, and 8 s. Each subject was trained to stability.

Data Analysis

Four parameters were tracked on a session-by-session basis: median latency-to-initiate trials (LTI), median IRT, the coefficient of quartile variation (CQV) of IRTs (difference between first and third quartile divided by their sum), and the number of obtained reinforcers (ORs). The acquisition phase of each parameter was defined as the mean performance during the first five sessions of each schedule, while the asymptote was defined as the mean during the last five sessions. ANOVAs were conducted to assess statistical significance of time and genotype on FMI schedule, and Student's *t*-tests were conducted to examine parameter differences based on genotype.

Data Availability

The manuscript and SI contain all data, often with representative images. The mouse lines, materials, protocols, biochemical, or imaging data are available upon reasonable request of the corresponding author.

Results

Expression of ERK/MAPK Components in Adult CINs

The ERK/MAPK cascade is dynamically activated during embryogenesis to varying degrees in most cell types. Neural progenitors in the embryonic ventricular zone typically show high levels of P-ERK1/2 relative to immature migrating postmitotic neurons (Stanco et al. 2014; Pucilowska et al. 2018), while in adult cortices, P-ERK1/2 labeling is highly enriched in a subset of excitatory PNs, especially in layer 2/3 (Cancedda et al. 2003; Pham et al. 2004; Suzuki et al. 2004; Gauthier et al. 2007; Xing et al. 2016; Holter et al. 2019). The RNA levels of *Mapk1/Erk2* and *Map2k1/Mek1* have been shown to be globally lower in GABAergic CINs relative to PNs in the visual cortex, but the expression and activation of ERK/MAPK signaling proteins have not been well characterized in CINs in vivo (Mardinly et al. 2016).

To indelibly label all CINs during development, we generated mice expressing *Slc32a1:Cre* (aka *VGAT:Cre* or *VIAAT:Cre*) and the Cre-dependent tdTomato/red fluorescent protein (RFP) reporter, Ai9, which showed the expected pattern of GABAergic neuron-directed RFP expression throughout the forebrain (Fig. 1A–D) (Madisen et al. 2010; Vong et al. 2011). Immunolabeling for MEK1/MAP2K1 and ERK2/MAPK1 revealed relatively lower expression in CINs in comparison to NEUN⁺/RFP[−] presumptive PNs (Fig. 1E–J). In agreement with previous studies, high levels of P-ERK1/2 were observed in a subset of NEUN⁺/RFP[−] PNs in cortical layer 2/3 (Fig. 1K–M, arrowheads) (Cancedda et al. 2003; Pham et al. 2004; Suzuki et al. 2004). However, P-ERK1/2 levels in RFP⁺ CINs were detectable, but qualitatively lower relative to this subset of surrounding PNs (Fig. 1K–M, dotted yellow outlines). These data extend past transcriptomic studies by showing that CINs express relatively lower protein levels of ERK2, MEK1, and P-ERK1/2 than excitatory neurons in cortical layer 2/3 and suggest potentially distinct functions for this cascade between these two primary cortical neuron subtypes.

GABAergic-Autonomous caMEK1 Expression Decreases PV-CIN Number

Increased activity in multiple RTK-linked cascades, including ERK/MAPK, is observed in many neural subtypes that express RASopathy-linked mutations (Tidyman and Rauén 2016). To selectively increase MEK1 signaling in specific neuronal populations, we utilized a Cre-dependent, constitutively active

CAG-Loxp-Stop-Loxp-Mek1^{S217/221E} (*caMek1*) allele, which has been shown to hyperactivate ERK1/2 signaling in multiple cell types (Alessi et al. 1994; Cowley et al. 1994; Klesse et al. 1999; Bueno et al. 2000; Krenz et al. 2008; Li et al. 2012; Lajiness et al. 2014). We generated *caMek1, Slc32a1:Cre* mice to overexpress caMEK1 in a GABAergic neuron-specific fashion during embryogenesis. *CaMek1, Slc32a1:Cre* mice were viable and grossly normal, though mutants exhibited larger average body mass than controls in adulthood. Significantly elevated MEK1 levels were clearly detectable in cells expressing the Cre-dependent RFP reporter in the E13.5 ganglionic eminence mantle zone and cortical migratory streams, as well as in adult CINs (Supplemental Fig. 1A–F, I–J).

Quantitative assessment of P-ERK1/2 protein levels in CINs via western blotting approaches is complicated by the low CIN frequency in a whole cortical lysate (~5 to 10% of all cortical cells). Previously, we utilized cortical PN-targeting *Nex/NeuroD6:Cre* mice to show that caMEK1 expression reduces corticospinal axon outgrowth, but not PN number (Xing et al. 2016). We quantified P-ERK1/2 levels in western blots of E14.5 *caMek1, Nex:Cre* cortical lysates, a time when PNs are maximally enriched in the developing cortex. *CaMek1, Nex:Cre* whole cortical lysates exhibit a modest, but statistically significant, 1.47 ± 0.2-fold increase in the levels of P-ERK1/2 in comparison to controls (Supplemental Fig. 1G,H). These data suggest *caMek1, Slc32a1:Cre* mice provide a model of hyperactive MEK1 signaling in GABAergic neurons from early stages of CIN development.

Surprisingly, assessment of fluorescently labeled CINs in adult *caMek1, Slc32a1:Cre, Ai9* sensory cortices revealed a significant reduction in total RFP⁺ cell density (Fig. 2A–I). CIN density appeared to be affected in multiple cortical regions, such as primary motor and auditory cortices (Supplemental Fig. 2A–L). In the adult sensory cortex, approximately 40% of CINs express PV, whereas 30% express SST, which serve as mostly nonoverlapping markers of two distinct populations of CINs (Rudy et al. 2011; Kelsom and Lu 2013; Kessarar et al. 2014). Strikingly, we observed a significant reduction in the proportion of PV⁺/RFP⁺ CINs, but not in the proportion of SST⁺/RFP⁺ CINs (Fig. 2J–P). We detected a significant decrease in RFP⁺ cells in cortical layers 1, 2–4, and 5, but not layer 6 (Fig. 2Q), while the density of PV-CINs was significantly decreased in layers 2–4, 5, and 6 (Fig. 2R). Finally, surviving mutant PV, but not SST, expressing CINs displayed a significant increase in somal area compared with control neurons in layers 2 and 5 (Fig. 2S–W).

Recombination in GABAergic neurons throughout the entire nervous system of *Slc32a1:Cre* mice left open the possibility that indirect caMEK-related changes in regions connected to the cortex, particularly the basal ganglia, could alter global cortical activity and noncell autonomously modulate PV-CIN number (Denaxa et al. 2018; Hutton et al. 2017; Kozorovitskiy et al. 2012). To reduce noncell autonomous contributions, we utilized *Nkx2.1:Cre*, which induces recombination in the early MGE and 60–80% of PV-CINs, in addition to nonneural derivatives (Xu et al. 2008). We generated *caMek1, Nkx2.1:Cre, Ai9* mice and assessed the proportion of PV⁺/RFP⁺ CINs. *CaMek1, Nkx2.1:Cre* mice exhibited generalized growth delay in the second–third postnatal week and were not viable past the first postnatal month (*n* = 8). We cannot exclude that caMEK1 effects on *Nkx2.1:Cre*-recombined cells outside of the nervous system, such as the lung or thyroid, might contribute to premature lethality. Nonetheless, consistent with our previous findings, P14 *caMek1, Nkx2.1:Cre, Ai9* mice displayed a significant reduction in PV⁺/RFP⁺-CIN density (Supplemental Fig. 2M–U). Finally, we

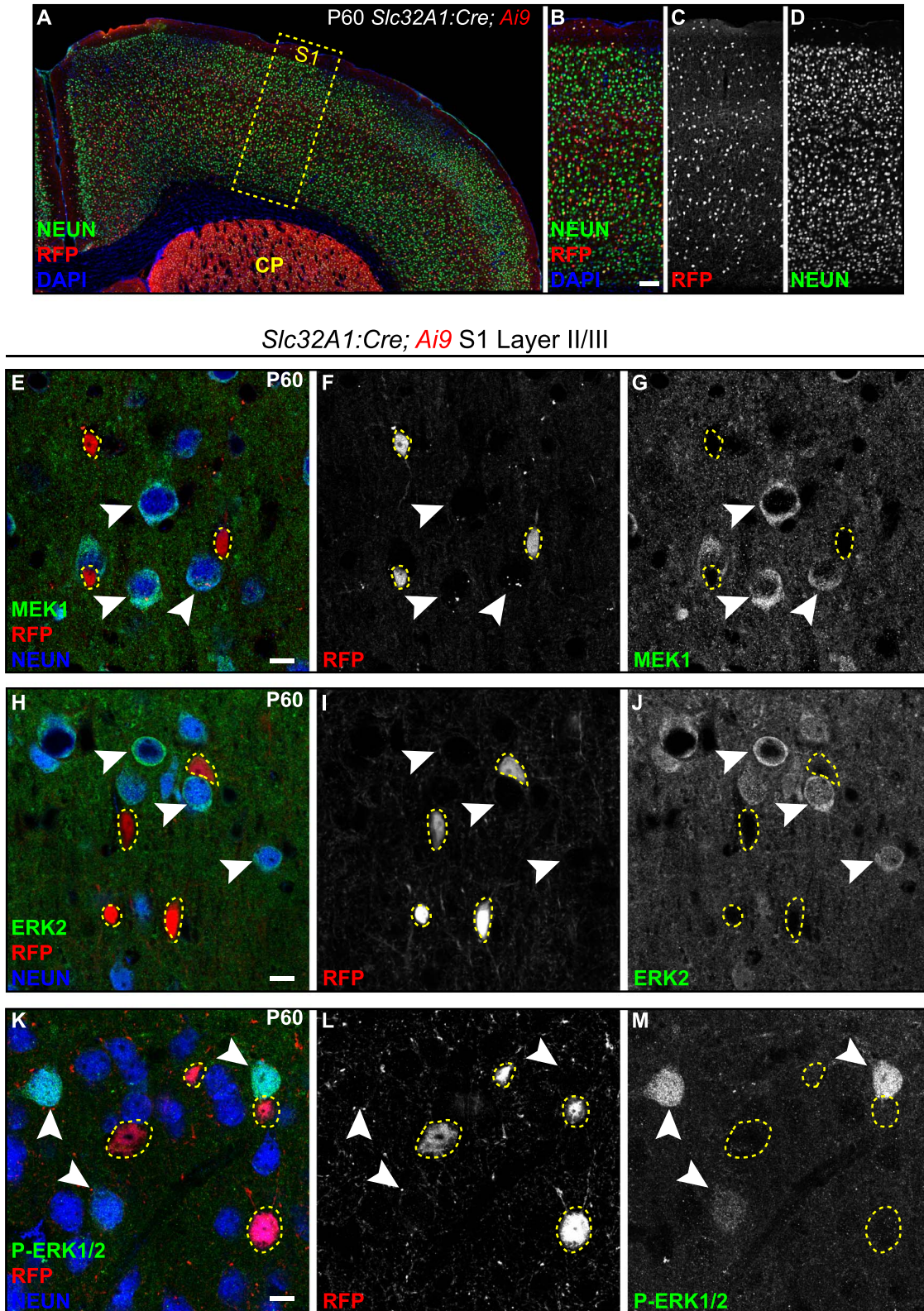


Figure 1. Cortical CINs exhibit low levels of ERK/MAPK expression and activity. (A–D) Representative confocal images of *Slc32A1:Cre, Ai9* sensorimotor cortex. Note the robust expression of RFP in brain regions with high densities of GABAergic neurons. (Scale bar = 100 μ m) (E–M) Immunolabeling for MEK1 (E–G) and ERK2 (H–J) showed comparatively low expression in inhibitory CINs (yellow outlines) when compared with NEUN⁺/Ai9⁻ presumptive PNs (arrowheads) in layer 2 ($n = 3$ mice). Relatively lower levels of P-ERK1/2 (K–M) was observed in inhibitory CINs when compared with PNs expressing high levels of P-ERK1/2 ($n = 3$ mice). (Scale bar = 10 μ m).

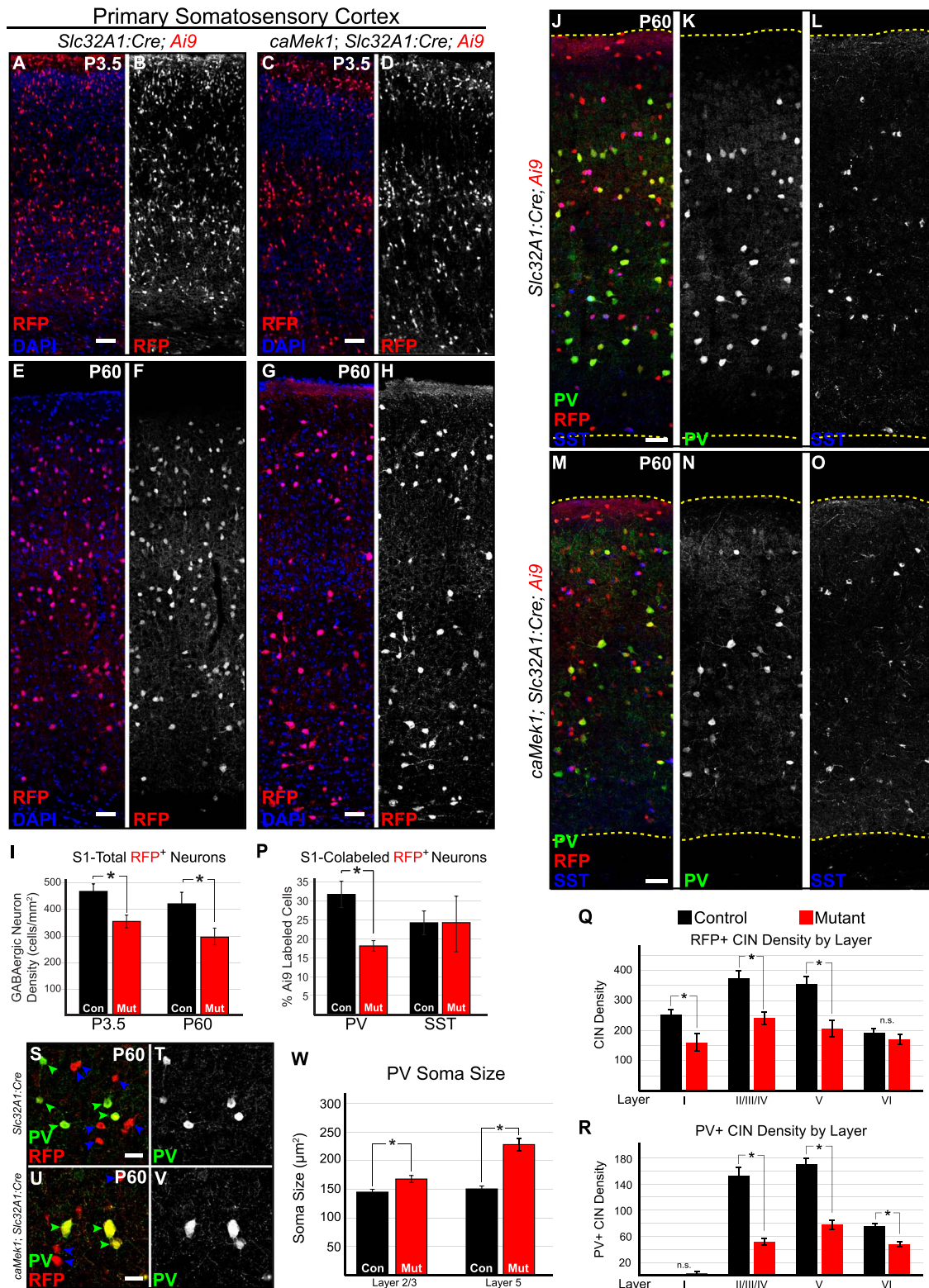


Figure 2. MEK1 hyperactivation leads to a selective reduction in PV-expressing CINs in the postnatal cortex. (A–I) *caMek1; Slc32A1:Cre; Ai9* mutant P3.5 (A–D) and P60 (E–H) primary somatosensory cortices exhibit reduced numbers of Ai9-expressing CINs in comparison to *Slc32A1:Cre; Ai9* controls (quantification in I, $n = 3$, mean \pm SEM, $*P < 0.05$). (Scale bar = 100 μm) (J–P) We quantified the proportion of fluorescently labeled PV+/RFP+ or SST+/RFP+ coexpressing CINs in the sensory cortex. Confocal micrographs of RFP-expressing CINs at P60 demonstrate that the proportion of PV+/RFP+ CINs, but not SST+/RFP+ CINs, was significantly decreased in mutants (M–O) in comparison to controls (J–L) (quantification in P, $n = 3$, mean \pm SEM, $*P < 0.05$) (Scale bar = 100 μm). (Q) We detected significant reductions in the density of RFP+ CINs in layers 1, 2–4, and 5, but not layer 6 ($n = 4$ controls, $n = 3$ mutants, mean \pm SEM, $*P < 0.05$). (R) The density of PV-expressing CINs was significantly reduced in layers 2–4, 5, and 6 ($n = 4$ controls and 3 mutants, mean \pm SEM, $*P < 0.05$). (S–W) Layer 5 mutant PV-CINs (U–V, green arrowheads) display increased soma size in comparison to control PV-CINs (S, T) (quantification in W, $n = 60$ neurons in each condition per layer, mean \pm SEM, $*P < 0.01$). RFP+ CINs lacking PV displayed no qualitative change in soma size (S, U, blue arrowheads). (Scale bar = 25 μm).

generated a *caMek1, Dlx5/6:Cre* strain that recombines in select neural crest and forebrain ganglionic eminence derivatives, including postmitotic CINs, and also observed a reduced density of PV-CINs (Supplemental Fig. 2V–Y) (Monory et al. 2006). In summary, these data suggest that the establishment of PV-CIN number is cell autonomously vulnerable to caMEK1 expression.

Increased Apoptosis of Immature Cortical Interneurons during Embryogenesis

RFP⁺ CIN density in P3.5 *caMek1, Slc32A1:Cre, Ai9* mice was significantly reduced, suggesting embryonic processes necessary to establish CIN number are disrupted by caMEK1 expression. Indeed, examination of RFP⁺ CIN density in the E17.5 cortical plate also revealed fewer CINs in *caMek1, Slc32A1:Cre, Ai9* embryos (Supplemental Fig. 3A–E). Analysis of mutant recombined striatal GABAergic neuron density did not reveal a significant difference from controls, suggesting the reduction in PV-CINs is not due to ectopic CIN migration into the striatum (data not shown). We next examined markers of neuronal death during early CIN migration in the E13.5 *caMek1, Slc32A1:Cre, Ai9* subpallium. Immunolabeling for the apoptotic marker cleaved caspase 3 (CC3) revealed colocalization with a subset of RFP⁺ neurons within the mantle zone of the ganglionic eminences in E13.5 mutant, but not control, embryos (Fig. 3A–F). Condensed, pyknotic nuclei were seen in CC3⁺/RFP⁺ neurons (Fig. 3G–J). We also observed CC3⁺/RFP⁺ cells with pyknotic nuclei in *caMek1, Nkx2.1:Cre, Ai9* mantle zones (Supplemental Fig. 3F). No CC3⁺/RFP⁺ cells were observed in the mutant cortical migratory streams in the dorsal pallium.

Expression of the ERK/MAPK effector, MEF2C, is enriched in the early PV-CIN lineage and promotes their establishment during development (Mayer et al. 2018). We tested whether alterations in MEF2C immunoreactivity could be detected in regions of the subpallial mantle zone that contain apoptotic neurons in mutant mice. We immunolabeled for MEF2C in E13.5 control mice and found that 9 of 120 RFP⁺ neurons in the LGE mantle zones coexpressed MEF2C (Fig. 3K–M, yellow arrowheads). In the developing *caMek1, Slc32A1:Cre, Ai9* LGE mantle zone, 7 of 120 RFP⁺ cells exhibited MEF2C⁺ colabeling (Fig. 3N–P, yellow arrowheads). Relatively higher levels of MEF2C were apparent in RFP⁺ CINs in the cortical migratory streams dorsal to the pallial/subpallial boundary. Together, our results suggest caMEK1-associated reductions in PV-CIN density result from the death of a subset of migrating CINs in the ganglionic eminence mantle zone independent of significant changes in MEF2C expression.

GABAergic-Specific *caMek1* Expression Promotes Cortical Hyperexcitability and Reduces Fast-Spiking CIN Intrinsic Excitability, without Altering the Development of a Fast-Spiking Phenotype

An increased risk of epilepsy and autism is observed in individuals with ERK/MAPK-linked genetic syndromes (Yoon et al. 2007; Digilio et al. 2011; Rauén et al. 2013). We tested whether MEK1 hyperactivation in GABAergic circuits using *Slc32A1:Cre* is sufficient to trigger behavioral changes associated with these conditions. We conducted a series of behavioral tests by first using the open field, then the elevated plus maze, and finally the social approach assay. No difference in global locomotor activity, anxiety-like behavior, or sociability could be detected (Supplemental Fig. 4A,B,D–I). We did not detect overt generalized tonic-clonic seizures in mutant mice while normally housed in home cages. However, during

the initial 60 s of open field testing with 13 adult *caMek1, Slc32A1:Cre* mutants, two mutant mice exhibited increased head twitching, aberrant locomotor activity, and increased rearing (Supplemental Video 1) and three mutant mice displayed periods of sudden behavioral arrest and motionless staring (Supplemental Video 2). These behaviors were not observed in any control mice. Consistent with these subtle impairments, closer examination of the first 10 s of the open field task revealed a significant reduction in distance traveled in *caMek1, Slc32A1:Cre* mice (Supplemental Fig. 4C).

We then performed intracortical EEG recordings to directly assess cortical activity, which revealed spontaneous epileptiform-like discharges in three of six *caMek1, Slc32A1:Cre* adult mice, but not control mice (Fig. 4A). We also found that the average threshold to seizure induction in response to PTZ administration in these six mutants was significantly reduced when compared with controls (Fig. 4B). Seizures have been shown to increase the local expression of glial fibrillary acidic protein (GFAP) in astrocytes (Steward et al. 1992; Stringer 1996). Three untested *caMek1, Slc32A1:Cre* mice exhibited clear clusters of GFAP-expressing astrocytes in the cortex consistent with local reactive astrogliosis near hyperexcitable foci (Fig. 4C,D). Since certain seizure-related phenotypes were not fully penetrant, we conclude that MEK1 hyperactivation in GABAergic neurons may be a potential risk factor for cortical hyperexcitability in this mouse model.

To determine if caMEK1 expression is sufficient to alter basic electrophysiological properties of CINs, we performed whole-cell patch clamp recordings on *caMek1, Nkx2.1:Cre, Ai9* mice between P21 and P23. We utilized the *Nkx2.1:Cre* strain due to its more restricted pattern of recombination in forebrain circuits relative to *Slc32A1:Cre* mice. PV-CINs provide a powerful source of inhibition in the cortex, firing action potentials at frequencies greater than 200 Hz, due in part to the unique expression of the fast-inactivating potassium channel Kv3.1, which begins in the second postnatal week (Rudy and McBain 2001; Okaty et al. 2009; Goldberg et al. 2011). Current clamp recordings of fluorescently labeled CINs revealed that both control ($n = 12$) and mutant ($n = 9$) neurons retained their distinctive electrophysiological fast-spiking phenotype (>200 Hz) (Fig. 4E) (Anderson et al. 2010; McCormick et al. 1985). In response to increasing levels of current injection, however, *caMek1, Nkx2.1:Cre* mutant FS-CINs displayed a marked decrease in firing frequency with an overall decrease in the F-I slope of over 70% (Fig. 4F, $P < 0.05$). Statistically significant increases in input resistance and action potential amplitude and a nonsignificant trend toward decreased rheobase ($P = 0.14$) were also observed (Fig. 4G–I). No significant differences were observed in resting membrane potential, adaptation index, or action potential threshold (Fig. 4G–I). The reduction in F-I slope and intrinsic excitability may diminish inhibitory drive and contribute to cortical hyperexcitability.

Inhibitory Synapse Formation and Perineuronal Net Accumulation Are Altered by MEK1 Hyperactivity

PV-expressing CINs preferentially innervate PNs, often forming synapses on the perisomatic domain (Chattopadhyaya et al. 2004). We assessed whether perisomatic VGAT-labeled synapses surrounding layer 2/3 PNs were diminished in adult *caMek1, Slc32A1:Cre, Ai3* mice. We found the extent of VGAT immunolabeling in the perisomatic space of NEUN⁺/GFP⁻ pyramidal neuron soma was significantly reduced in mutant cortices when compared with controls (Fig. 5A–F,M). Interestingly, the area of

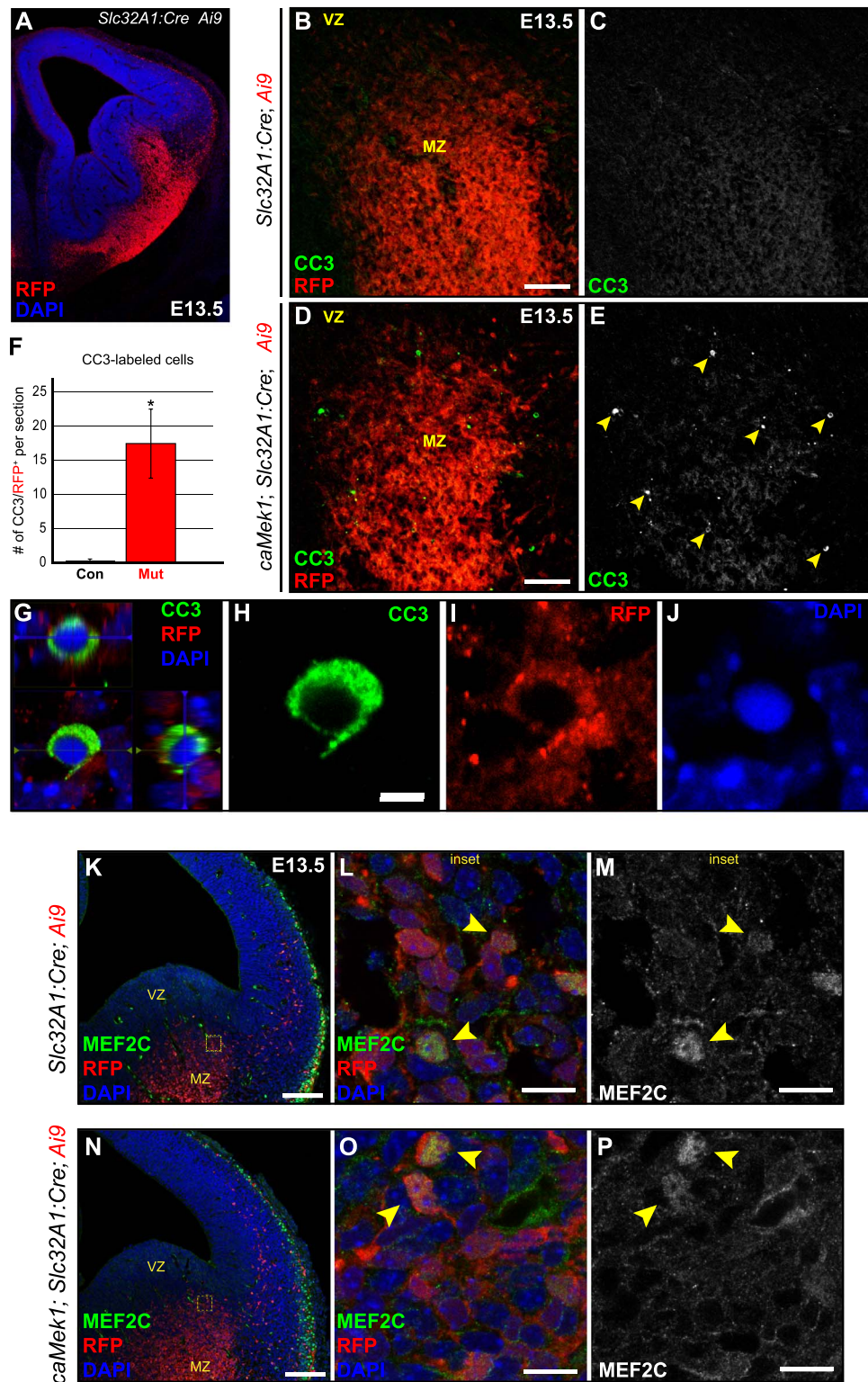


Figure 3. A subset of immature GABAergic neurons undergoes cell death during midembryogenesis. (A) E13.5 coronal section of RFP-labeled CINs in the mantle zones of the *Slc32A1:Cre* subpallium during midembryogenesis. (B–E) Immunolabeling for cleaved caspase 3 (CC3) showed a significant increase in the number of apoptotic profiles in *caMek1, Slc32A1:Cre, Ai9* mutants (D–E) as compared with controls (B,C) (quantification in F, $n = 3$, mean \pm SEM, $*P < 0.05$). Cell death was confined to the mantle zones of the subpallium (MZ) and no apoptotic profiles were observed in the dorsal pallial migratory streams. (Scale bar = 100 μ m) (G–J) Representative confocal z-stacks of CC3-labeled cells from *caMek1, Slc32A1:Cre, Ai9* embryos (G–J, Scale bar = 2 μ m) show clear colocalization with RFP and a condensed, pyknotic nuclear morphology. (K–P) Immunolabeling for MEF2C revealed enriched expression in RFP⁺ CINs within the cortical migratory streams relative to RFP⁺ cells in the lateral mantle zone. No significant change in the proportion of MEF2C⁺/RFP⁺ cells was observed in *caMek1, Slc32A1:Cre, Ai9* LGE mantle zone relative to controls (yellow arrowheads, $n = 3$ embryos per condition) (K, N—scale bar = 200 μ m, L, M, O, P—scale bar = 10 μ m).

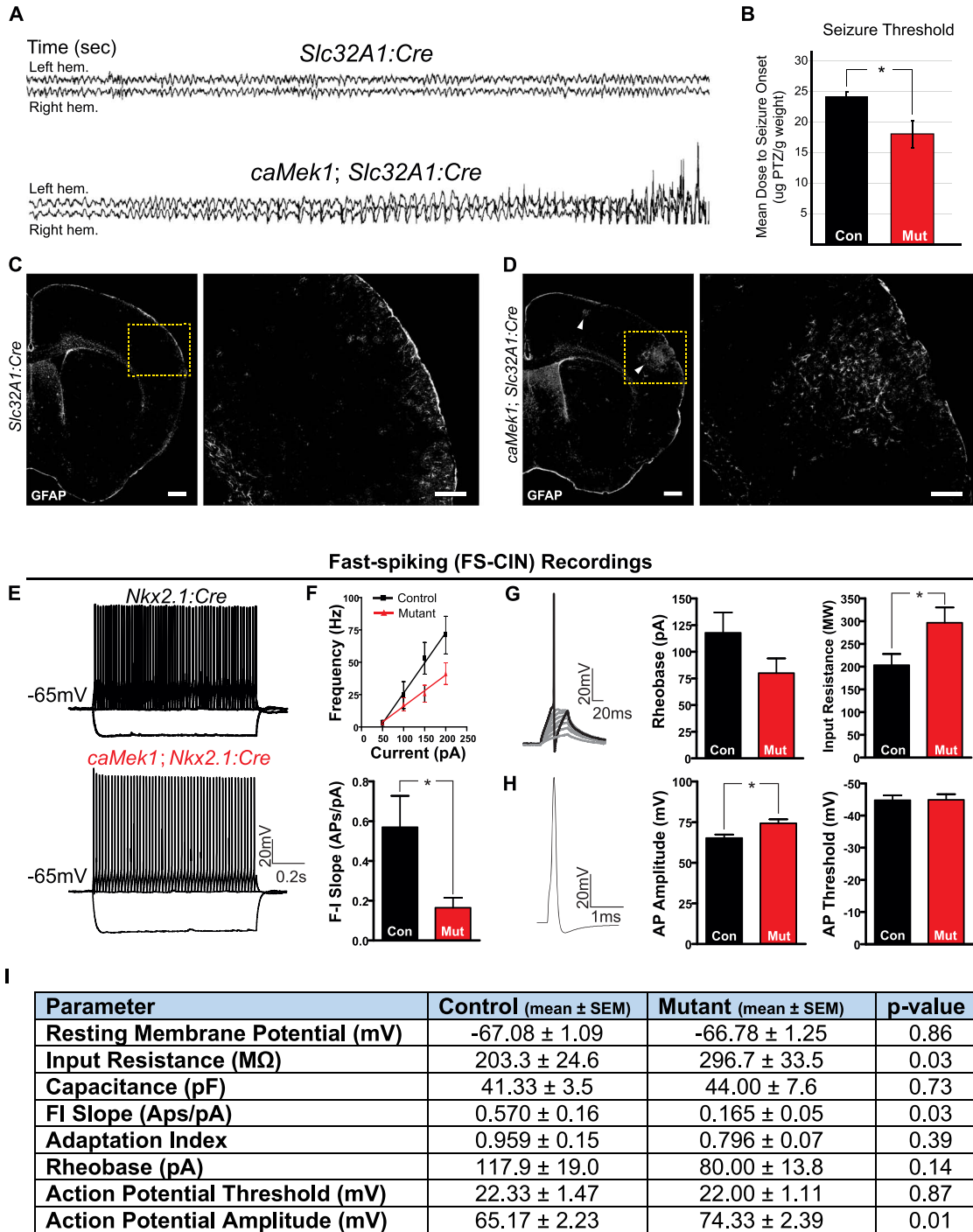


Figure 4. *caMek1 Slc32A1:Cre* CINs maintain typical fast-spiking properties, but a subset of mice exhibits seizure-like phenotypes. (A) Representative traces from forebrain-penetrating EEG revealed epochs of synchronous firing in 3 of 6 *caMek1 Slc32A1:Cre*, but not control mice. (B) Tail vein PTZ injections revealed a significant reduction in mean dose to seizure onset of PTZ ($n=6$, mean ± SEM, $*P < 0.001$). (C,D) *caMek1 Slc32A1:Cre* cortices display aberrant clusters of GFAP-labeled astrocytes (D arrowheads) that were not observed in controls (C) ($n=3$) (Scale bar = 100 μm). (E) Representative current clamp recordings of FS CINs in P21–23 *Nkx2.1:Cre Ai9* and *caMek1 Nkx2.1:Cre Ai9* mutant cortices. (F) Mutant CINs had a significantly reduced FI slope in comparison to controls (mean ± SEM, $P < 0.05$). (G,H) Representative current clamp recordings during rheobase (G) or single action potential (H) protocols. While a decreased trend was observed in rheobase ($P = 0.14$), significant increases were observed in input resistance and action potential amplitude (mean ± SEM, $*P < 0.05$). (I) Table of the intrinsic electrophysiological properties of fast-spiking CINs from *caMek1 Nkx2.1:Cre Ai9* mice.

VGAT labeling in the surrounding neuropil, typically innervated by SST-CINs, was unchanged (Supplemental Fig. 5A–E). These data suggest that PV-CIN inhibitory output is selectively vulnerable to caMEK1 signaling, while SST-CINs are less affected.

PV-CINs selectively accumulate an extracellular structure called the perineuronal net (PNN) derived primarily from glial chondroitin sulfate proteoglycans (CSPGs). PNNs are essential to cortical development, restricting plasticity during the closure of critical periods and protecting PV-CINs from oxidative stress associated with a high-frequency firing rate (Hensch 2005b; Cabungcal et al. 2013). Reductions in PNN formation have been found in multiple models of neurodevelopmental disorders that exhibit loss of PV-CINs (Cabungcal et al. 2013; Bitanirwe and Woo 2014; Krencik et al. 2015; Krishnan et al. 2015; Steullet et al. 2017). We utilized WFA labeling to test whether PNN formation was reduced in adult *caMek1*, *Slc32A1:Cre*, *Ai3* mice (Fig. 5G–L). In both control and mutant mice, >85% of PV-expressing cells exhibited significant WFA labeling, and PNNs were rarely detected on CINs that lacked PV expression. This suggests caMEK1 expression had little effect on the specification of cellular programs required for PNNs in surviving PV-CINs. Surprisingly, we found that surviving mutant PV-CINs had significantly brighter WFA⁺ PNNs relative to controls (Fig. 5G–L). Consistent with the larger somal size of mutant PV-CINs, the cross-sectional area of WFA-labeled profiles was significantly increased (Fig. 5N). Analysis of the quantitative level of WFA labeling in mutant PV-CINs across layers 2–5 revealed a robust increase in PNN accumulation as compared with controls (Fig. 5O). Mutant WFA-labeled CINs exhibited normal expression of 8-oxo-2'-deoxyguanosine (8-oxo-dg), a marker of DNA oxidation often altered in neurons with reduced PNNs (Supplemental Fig. 5F–I) (Steullet et al. 2017). Collectively, MEK1 hyperactivation clearly increases PNN accumulation but does not trigger ectopic PNN formation on GABAergic neurons lacking PV.

caMek1, Slc32A1:Cre Mice Display Delayed Acquisition of a Behavioral Response Inhibition Task

ADHD is associated with altered prefrontal cortex (PFC) function and a significant proportion of syndromes linked to abnormal ERK/MAPK activity (Adviento et al. 2014; Garg et al. 2013; Green et al. 2017; Pierpont et al. 2018; Walsh et al. 2013; Gabay et al. 2018). Individuals with ADHD often exhibit structural changes in the PFC, a region associated with the inhibition of reinforced responses (Seidman et al. 2006). PFC-associated cognitive deficits have been identified in a mouse model of fragile X syndrome (Krueger et al. 2011), but the effects of GABAergic-specific MEK1 hyperactivity on PFC function is unknown. As observed in other cortical regions, we noted a significant $38.69 \pm 12.1\%$ (mean \pm SEM, $n = 3$, $P < 0.05$) reduction in total CIN density in the mPFC of *caMek1*, *Slc32A1:Cre*, *Ai9* mice (Fig. 6A–F). To examine response inhibition directly, we utilized an FMI test, a timing-based task that requires animals to withhold a response for a fixed period. This paradigm is perhaps more favorable than the five-choice serial reaction time task (5-CSRTT) and differential reinforcement of low rates task (DRL), because the self-paced design dissociates response inhibition capacity from motivational aspects of behavior (Doughty and Richards 2002; Bizarro et al. 2003; Hill et al. 2012; Watterson et al. 2015). Here, adult control and *caMek1*, *Slc32A1:Cre* mice were trained to initiate trials via a nose-poke, which resulted in the presentation of sweetened condensed milk in the reward receptacle. Mice were

then placed on an FMI schedule, where a time delay between the initiating nose-poke and the availability of reinforcement in the reward receptacle was implemented (Fig. 6G). Reward was delivered only if the time between the initiating nose-poke and attempt to obtain reward (IRT) exceeded a predetermined withholding period. If mice prematurely accessed the reward receptacle, no reward was delivered.

Following initial training on an FMI with a very short (0.5 s) response-withholding period, we measured mouse performance when the withholding period was extended to 2 s, 4 s, and, finally, 8 s. We observed a main effect of FMI schedule irrespective of genotype, such that IRTs increased as the FMI withholding period increased ($F(2, 62) = 535.12$, $P < 0.01$). Importantly, mutants showed clear evidence of impaired acquisition of the FMI task. We found a main effect of genotype on the mean median IRT during the first 5 days of each FMI schedule (acquisition period), in which mutant mice had relatively lower IRTs compared with control mice ($F(1, 62) = 18.73$, $P < 0.01$) (Fig. 6H). In further support of reduced response inhibition capacity, mutant mice exhibited increased variability in their IRTs as measured by the coefficient of quartile variation (CQV) during acquisition ($F(1, 62) = 31.73$, $P < 0.01$) and asymptotic performance (defined as the last 5 days of the FMI) ($F(2, 62) = 5.055$, $P < 0.001$) across all schedules (Fig. 6I). Median IRTs during the asymptotic phase in mutants and controls were not statistically different in any schedule (Fig. 6H inset). Thus, these data suggest that mutant mice are capable of learning to inhibit reinforced responses for up to 4 s but show a significant delay in acquiring this capability.

Due to *Slc32A1:Cre*-mediated recombination within subcortical circuitry, it is possible that altered reward pathway activity influenced FMI performance. The latency to initiate (LTI) a trial provides a measure of motivation; for example, rats administered amphetamine show a reduction in LTI in a related task (Rojas-Leguizamón et al. 2018). However, we noted that mutants did not differ from controls in the median LTI at 2 and 4 s, indicating that motivation to obtain rewards was not significantly altered between conditions (Tukey's *b* post hoc test—2 s: $t(21) = 1.39$, $P = 0.18$; 4 s: $t(21) = -0.29$, $P = 0.77$) (Fig. 6J). We found that during the 8-s FMI, mutant mice exhibited a statistically significant increase in LTI ($t(20) = 2.43$, $P < 0.05$) (Fig. 6J). This apparent loss of motivation at the 8-s FMI is likely due to the fact that the mean median asymptotic IRT did not reach the 8-s criterion even after 32 days of testing (control: 8.45 ± 1.04 ; mutant: 7.26 ± 1.09) and is also consistent with the statistically significant reduction in mean obtained reinforcers at the 8-s FMI (Fig. 6K). Collectively, our data indicate that caMEK1 effects on GABAergic circuits impair the acquisition of response inhibition capacity and may be linked to cognitive abnormalities in RASopathy individuals.

Discussion

Here, we show that GABAergic neuron-autonomous MEK1 hyperactivation is associated with the death of a subset of immature GABAergic neurons in the mouse embryonic subpallium and a selective reduction in PV-CIN density, but not SST-CINs, in adulthood. These mutants exhibit a significant reduction in perisomatic GABAergic synapses on layer 2/3 PNns that coincided with an increased risk of mild seizure-like activity. Surviving *caMek1*-expressing PV-CINs retained their characteristic FS phenotype but show a significantly reduced firing output and an unexpected increase in the extent of PNN accumulation. Mutant mice displayed relatively

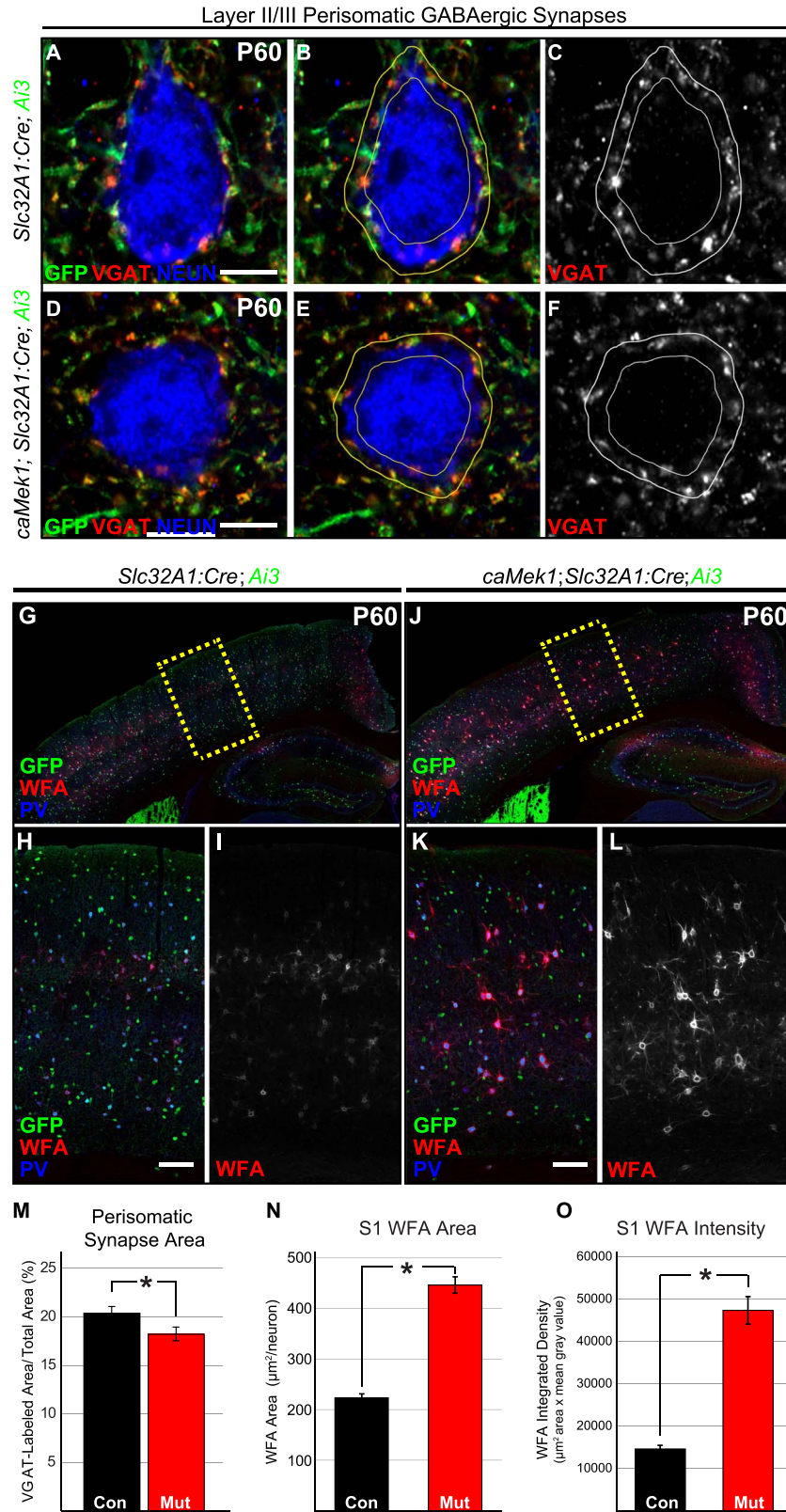


Figure 5. Reduced perisomatic synapse labeling in mutant cortices coincides with a substantial increase in PNN formation on PV-CINs. (A–F) Representative high-resolution confocal Airyscan images of triple immunolabeled cortical sections for Ai3, VGAT, and NEUN. Excitatory neuron perisomatic domains were outlined and quantification of VGAT-labeled pixels revealed that mutants (D–F) have a significant reduction in the amount of perisomatic VGAT labeling (Scale bar = 3 μm) in comparison to controls (A–C) (quantification in M; $n = 48$ control, 53 mutant neurons; mean \pm SEM, $*P < 0.05$). (G–L) P60 representative coronal sections of *Slc32A1:Cre Ai3* (G–I) and *caMek1 Slc32A1:Cre Ai3* (J–L) cortices immunolabeled for GFP, WFA, and PV. The WFA labeling was imaged using the same acquisition settings for all samples. A significant increase in WFA-labeled area per neuron (N) and WFA-labeling intensity (O) was detected in mutant PV⁺ CINs when compared with controls ($n = 60$ control, 60 mutant neurons, mean \pm SEM, $*P < 0.001$) (Scale bar = 100 μm).

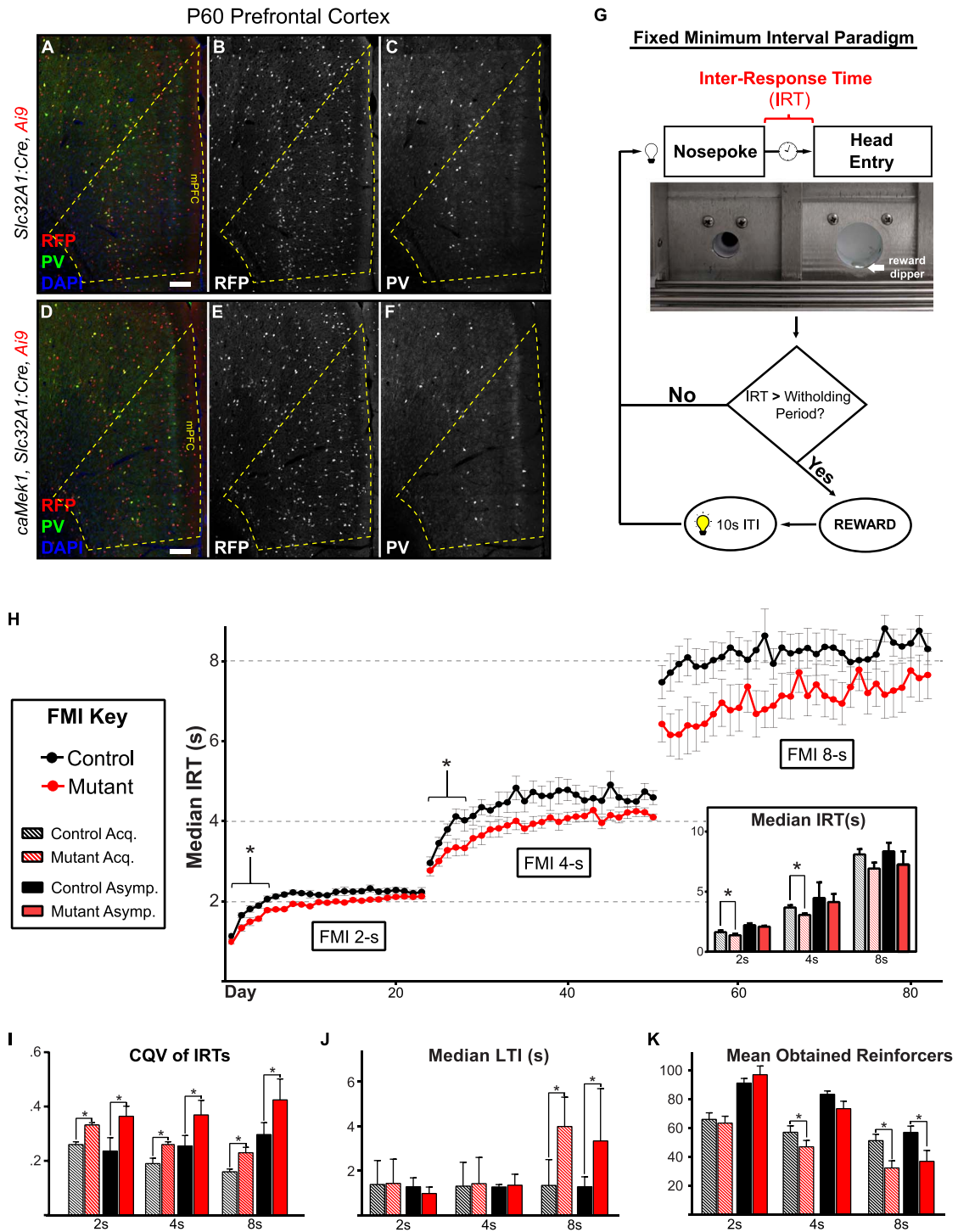


Figure 6. caMEK1 Slc32A1:Cre mice exhibit reduced behavioral response inhibition capacity. (A–F) The mutant mPFC exhibits a decrease in RFP⁺ and PV⁺ CINs (D–F) relative to controls (A–C) ($n = 3$). (Scale bar = 100 μ m) (G) Schematic of the FMI task. (H) Mutant mice had a significant reduction in mean median IRT during FMI acquisition in 2- and 4-s schedules ($n = 12$, mean \pm SEM, * $P < 0.05$). (I) Mutant mean CQV of IRTs during both acquisition and asymptotic phases was significantly increased in 2-, 4-, and 8-s FMI schedules (mean \pm SEM, * $P < 0.05$). (J) Median acquisition and asymptotic LTI were significantly increased in the 8-s FMI, but not in the 2- and 4-s schedules (mean \pm SEM, * $P < 0.05$). (K) Mutant mice had a reduction in mean acquisition ORs at 4 s and a significant reduction in both mean acquisition and asymptotic ORs during the 8-s FMI (mean \pm SEM, * $P < 0.05$).

normal performance in assays of locomotion, sociability, and anxiety, but deficits in the acquisition of behavioral response inhibition. These data suggest that GABAergic neuron-autonomous developmental defects might partly contribute to seizure risk and cognitive deficits in syndromes characterized by pathological activation of ERK/MAPK.

While the expression of ERK/MAPK pathway components is widespread, our findings reinforce the notion that levels are variable and pathway activation dynamics may vary between neural subtypes. We have extended past cell-specific transcriptional experiments to show that protein levels of ERK2 and MEK1 are lower in CINs than in surrounding PNs, which may be linked to the relative reduction in high P-ERK1/2-expressing CINs (Mardinly et al. 2016). Quantitative phosphoprotein analyses of low expressed targets in rare cell types *in vivo* pose a number of technical challenges. Additional semiquantitative studies of pan and phosphorylated-ERK1/2 levels *in vivo* using multiplexed immunohistochemical amplification at different developmental stages in distinct GABAergic subtypes may assist in defining context-dependent ERK/MAPK functions. Past work has shown that experience-dependent transcriptional responses in V1 PV-CINs are constrained relative to PNs (Hrvatín et al. 2018). A more stringent degree of ERK/MAPK recruitment in CINs might contribute to this reduced activity-dependent transcriptional response and certain CIN-specific functional properties (Tyssowski et al. 2018).

Defects in GABAergic circuitry have been implicated in the pathogenesis of Rett, fragile X, schizophrenia, and many other neurodevelopmental diseases (Cui et al. 2008; Chao et al. 2010; Steullet et al. 2017). Reduced PV-CIN number is often observed; however, the mechanism of loss is not always clear (Steullet et al. 2017). We show that MEK1 hyperactivation is sufficient to promote the GABAergic-neuron autonomous activation of caspase-3 and death of a subset of immature neurons in the embryonic ganglionic eminences. It will also be important to determine whether abnormal migration, perturbation of postnatal phases of CIN development, or some degree of ongoing neuronal death in aged mice further contribute to the reduced PV-CIN density in mutants. ERK/MAPK signaling is typically linked to cell survival, but death by sustained ERK/MAPK activity has been described in certain cellular contexts (Cagnol and Chambard 2010; Martin and Pognonec 2010). Sustained ERK/MAPK activity has been previously shown to drive proapoptotic cytochrome c release from mitochondria and mitochondrial physiology in distinct contexts (Cagnol and Chambard 2010). PV-CINs exhibit significantly higher densities of mitochondria in comparison to other neurons, such as SST-CINs and PNs, presumably to sustain the metabolic demand necessary for their fast-spiking properties (Inan et al. 2016; Paul et al. 2017). Thus, it is possible that the relatively selective loss of PV-CINs instead of SST-CINs in response to caMEK1 expression is related to an increased reliance on ERK1/2-dependent mitochondrial processes. Further research will be essential to establish mitochondrial dysfunction as a primary mechanism driving PV-CIN apoptosis during embryonic development. The reduction in PV-CIN density, but not SST-CIN density, in the postnatal cortex suggests some of the early dying neurons were committed to the PV lineage. The development of reliable embryonic markers for the PV-CIN lineage would be helpful for directly addressing this question *in vivo*.

Notably, *caMek1* expression in cortical excitatory neurons has not been associated with significant PN loss during development (Nateri et al. 2007; Xing et al. 2016). Our data hint at particularly

selective roles for kinase signaling networks at an early stage of CIN lineage differentiation. Clarifying why PV-CINs are particularly sensitive to pathological ERK/MAPK activity could be of therapeutic relevance to various neurodevelopmental conditions (Fowke et al. 2018). It will be interesting to evaluate whether treatment with pharmacological MEK1/2 inhibitors is capable of sustained restoration of CIN number in *caMek1*, *Slc32A1:Cre* mice.

In addition to the loss of a subset of PV-CINs, we also observed a modest yet significant reduction in RFP⁺ CINs lacking PV in layer 1 of adult *caMek1*, *Slc32A1:Cre* cortices. Approximately 90% of CINs that populate layer 1 are 5HT3AR-expressing neurogliaform cells derived from the CGE with known roles in the function of mature cortical circuits (Miyoshi et al. 2010; Rudy et al. 2011; Fu et al. 2014). Thus, loss of this important cell population may also be a contributing factor to aspects of RASopathy neuropathology. Future studies using CGE-directed conditional lines, such as 5HT3AR:Cre, would be useful for directly testing this possibility.

Despite the effect of caMEK1 on early GABAergic neuron survival, the physiological maturation of *caMek1*-expressing PV-CINs was not significantly impeded. Surviving mutant PV-CINs retained a characteristic fast-spiking signature with numerous electrophysiological properties remaining relatively unchanged. However, mutant PV-CINs displayed a marked decrease in their intrinsic responsiveness as indicated by a greater than 70% decrease in the slope of their induced firing rate. Input resistance and action potential amplitude were also observed to be increased in mutant PV-CINs, which could compensate for the loss of FS output. Nonetheless, we noted a modest, but statistically significant, decrease in perisomatic inhibitory synapse number on cortical PNs in mutant mice. As might be expected, a subset of mutant animals exhibited forebrain hyperexcitability and sudden behavioral arrest similar to previous reports in animal models of mild seizures. Overall, our findings indicate that MEK1 hyperactivation in developing GABAergic neurons increases the risk of subsequent cortical hyperexcitability.

The PNN is a critically important structure involved in the maturation of cortical circuitry with an important role in protecting PV-CINs from oxidative stress and limiting synaptic plasticity (Hensch 2005a; Hensch 2005b; Cabungcal et al. 2013; Morishita et al. 2015). Mouse models of schizophrenia, fragile X, and ASDs often exhibit reduced PV-CIN number and typically display a reduction in PNN formation (Steullet et al. 2017). In these models, increased oxidative stress is frequently observed in surviving PV-CINs. Increased PNN accumulation in the hyperactive MEK1 cortex may further shield PV-CINs from metabolic stressors. In support of this, we did not detect a change in the levels of PV-CIN 8-oxo-dg, a marker of oxidative stress. PV-CINs accumulate extracellular PNNs derived primarily from astrocyte-produced CSPGs (Galtrey and Fawcett 2007; Sorg et al. 2016). RASopathic astrocytes upregulate secreted ECM-associated CSPGs and promote an increase in the extent of PNN accumulation around PV-CINs (Krencik et al. 2015). Our data are the first to indicate a GABAergic-neuron autonomous role for enhanced PNN accumulation in response to MEK1 hyperactivation. The mechanism of enhanced PNN accumulation around PV-CINs is still under investigation. Increased MEK1 activity may drive a significant increase in PV-CIN-specific secreted molecules necessary to stimulate CSPG release from astrocytes. Alternatively, increased expression of hyaluronan synthase, an enzyme important in linking PNN components in the extracellular space, may drive enhanced accumulation of the PNN. Further CIN-specific transcriptional and functional validation studies

will be necessary to test these possibilities. It is thought that increased PNN accumulation on PV-CINs limits the plasticity of cortical regions and that the PNN may play a significant role in seizure susceptibility (Pizzorusso et al. 2002; McRae and Porter 2012). Similar to our findings, a recent report implicates changes in the PNN in altering intrinsic and firing properties of peritumoral FS and PN neurons (Tewari et al. 2018). Whether modification of PNN levels is capable of reversing the impaired cognitive function and intellectual disability frequently reported in RASopathy model systems is unknown but may be interesting to test in *caMEK1, Slc32a1:Cre* mice (Tidyman and Rauen 2016).

In addition to intellectual disability, ADHD is frequently diagnosed in Noonan syndrome and NF1, two common RASopathies (Miguel et al. 2015; Pierpont et al. 2018; Johnson et al. 2019). We examined cognitive phenotypes in *caMek1, Slc32A1:Cre* mice by assessing behavioral response inhibition capacity with an FMI-based task (Watterson et al. 2015; Rojas-Leguizamón et al. 2018). We detected significant deficits in the acquisition of response inhibition-dependent behaviors in mutant mice. It is plausible that this deficit is due to the reduced plasticity of PFC GABAergic circuitry in response to heightened levels of PNN or GABAergic-dependent changes in PN development (Cancedda et al. 2007). Since the entire GABAergic system is recombined in *Slc32a1:Cre* mice, it is possible *caMEK1* regulation of subcortical structures remains to be discovered that contribute to the cellular and behavioral phenotypes observed in this strain. In the least, our data show that GABAergic-directed MEK1 hyperactivation is sufficient to drive deficits in behavioral response inhibition, a cognitive process that may be linked to ADHD-like behaviors (Green et al. 2017).

Mutations in “upstream” RASopathy genes modulate a broader set of downstream cascades when compared with mutations in *Raf* or *Mek1/2*. *Nf1*, *Ptpn11/Shp2*, and *Syngap1* mutations result in a complex constellation of cellular changes, some of which depend upon ERK/MAPK modulation, whereas others have been shown to require signaling changes in PI3K, cAMP, and additional pathways (Brown et al. 2012; Anastasaki and Gutmann 2014). In combination with the recent finding that NF1 modulates PV-CIN specification, PV-CIN development may be particularly sensitive to signaling via NF1 and ERK/MAPK (Angara et al. 2020). Further analysis of forebrain GABAergic circuit development in syndromes linked to abnormal ERK/MAPK hyperactivation may be beneficial for identifying candidate mechanisms of epilepsy and cognitive defects.

Supplementary Material

Supplementary material can be found at *Cerebral Cortex* online.

Funding

National Institute of Health (grants R00NS076661 and R01NS097537 awarded to J.M.N., R01NS087031 awarded to T.R.A., and R01NS031768 to W.D.S.).

Author Contributions

Conceptualization: J.M.N., W.D.S., M.C.H., C.W.D., F.S., and T.R.A. Methodology: J.M.N., W.D.S., M.C.H., C.W.D., F.S., T.R.A., S.M., and D.M.T. Investigation: J.M.N., W.D.S., M.C.H., L.T.H., K.J.N., S.J.K., G.R.B., S.S., N.R.F., K.P.R., T.A.G., G.L., M.F.O., C.W.D., F.S., T.R.A., S.M., and D.M.T. Writing—Original Draft: M.C.H., J.M.N., C.W.D.,

T.A.G., F.S., T.R.A., S.M., M.F.O., L.T.H., and K.J.N. Writing—Review & Editing: M.C.H., J.M.N., G.R.B., S.J.K., S.S., N.R.F., K.P.R., and D.M.T. Funding Acquisition: J.M.N. and W.D.S. Resources: J.M.N., T.R.A., W.D.S., D.M.T., M.F.O., and F.S. Supervision: J.M.N., W.D.S., D.M.T., T.R.A., F.S.

Notes

We would like to thank Johan Martinez, Sam Lusk, Julia Pringle, Anna Kreuger, Sarah Sparks, Katie Riordan, Danielle Gonzalez, Elise Bouchal, and Kimberly Holter for their technical contributions to this work. *Conflict of Interest:* The authors declare no competing interests.

References

- Adviento B, Corbin IL, Widjaja F, Desachy G, Enrique N, Rosser T, Risi S, Marco EJ, Hendren RL, Bearden CE et al. 2014. Autism traits in the Rasopathies. *J Med Genet.* 51(1):10–20.
- Alessi DR, Saito Y, Campbell DG, Cohen P, Sitanandam G, Rapp U, Ashworth A, Marshall CJ, Cowley S. 1994. Identification of the sites in map kinase kinase-1 phosphorylated by p74raf-1. *EMBO J.* 13(7):1610–1619.
- Anastasaki C, Gutmann D. 2014. Neuronal *nf1/ras* regulation of cyclic amp requires atypical *pkc* activation. *Hum Mol Genet.* 23(25):6712–6721.
- Anderson TR, Huguenard JR, Prince DA. 2010. Differential effects of Na⁺-K⁺ ATPase blockade on cortical layer V neurons. *J Physiol.* 588(Pt 22):4401–4414.
- Angara K, Pai EL, Bilinovich SM, Stafford AM, Nguyen JT, Li KX, Paul A, Rubenstein JL, Vogt D. 2020. *Nf1* deletion results in depletion of the *Lhx6* transcription factor and a specific loss of parvalbumin⁺ cortical interneurons. *Proc Natl Acad Sci U S A.* 117(11):6189–6195.
- Aoidi R, Houde N, Landry-Truchon K, Holter M, Jacquet K, Charon L, Krishnaswami S, Yu B, Rauen K, Bisson N et al. 2018. *Mek1(Y130C)* mice recapitulate aspects of human cardio-facio-cutaneous syndrome. *Dis Model Mech.* 11(3).
- Bae MH, Bissonette GB, Mars WM, Michalopoulos GK, Achim CL, Depireux DA, Powell EM. 2010. Hepatocyte growth factor (HGF) modulates gabaergic inhibition and seizure susceptibility. *Exp Neurol.* 221(1):129–135.
- Berryer MH, Chattopadhyaya B, Xing P, Riebe I, Bosoi C, Sanon N, Antoine-Bertrand J, Lévesque M, Avoli M, Hamdan FF et al. 2016. Decrease of *Syngap1* in GABAergic cells impairs inhibitory synapse connectivity, synaptic inhibition and cognitive function. *Nat Commun.* 7:13340.
- Bitanhirwe BK, Woo TU. 2014. Perineuronal nets and schizophrenia: the importance of neuronal coatings. *Neurosci Biobehav Rev.* 45:85–99.
- Bizarro L, Murtagh C, Stolerman I. 2003. Differing effects of nicotine, amphetamine and caffeine on performance of a 5-choice serial reaction time task. *J Psychopharmacol.* 17(3): A31–A31.
- Brown J, Diggs-Andrews K, Gianino S, Gutmann D. 2012. Neurofibromatosis-1 heterozygosity impairs CNS neuronal morphology in a cAMP/PKA/ROCK-dependent manner. *Mol Cell Neurosci.* 49(1):13–22.
- Bueno OF, De Windt LJ, Tymitz KM, Witt SA, Kimball TR, Klevitsky R, Hewett TE, Jones SP, Lefer DJ, Peng CF et al. 2000. The *Mek1-Erk1/2* signaling pathway promotes compensated cardiac hypertrophy in transgenic mice. *EMBO J.* 19(23):6341–6350.

- Cabungcal JH, Steullet P, Morishita H, Kraftsik R, Cuenod M, Hensch TK, Do KQ. 2013. Perineuronal nets protect fast-spiking interneurons against oxidative stress. *Proc Natl Acad Sci U S A*. 110(22):9130–9135.
- Cagnol S, Chambard JC. 2010. Erk and cell death: mechanisms of ERK-induced cell death–apoptosis, autophagy and senescence. *FEBS J*. 277(1):2–21.
- Cancedda L, Putignano E, Impey S, Maffei L, Ratto GM, Pizzorusso T. 2003. Patterned vision causes Cre-mediated gene expression in the visual cortex through PKA and ERK. *J Neurosci*. 23(18):7012–7020.
- Cancedda L, Fiumelli H, Chen K, Poo M. 2007. Excitatory GABA action is essential for morphological maturation of cortical neurons in vivo. *J Neurosci*. 27(19):5224–5235.
- Chao HT, Chen H, Samaco RC, Xue M, Chahrouh M, Yoo J, Neul JL, Gong S, Lu HC, Heintz N et al. 2010. Dysfunction in GABA signalling mediates autism-like stereotypies and Rett syndrome phenotypes. *Nature*. 468(7321):263–269.
- Chattopadhyaya B, Di Cristo G, Higashiyama H, Knott GW, Kuhlman SJ, Welker E, Huang ZJ. 2004. Experience and activity-dependent maturation of perisomatic gabaergic innervation in primary visual cortex during a postnatal critical period. *J Neurosci*. 24(43):9598–9611.
- Clement JP, Aceti M, Creson TK, Ozkan ED, Shi Y, Reish NJ, Almonte AG, Miller BH, Wiltgen BJ, Miller CA et al. 2012. Pathogenic Syngap1 mutations impair cognitive development by disrupting maturation of dendritic spine synapses. *Cell*. 151(4):709–723.
- Cowley S, Paterson H, Kemp P, Marshall CJ. 1994. Activation of map kinase kinase is necessary and sufficient for PC12 differentiation and for transformation of nih 3t3 cells. *Cell*. 77(6):841–852.
- Cui Y, Costa R, Murphy G, Elgersma Y, Zhu Y, Gutmann D, Parada L, Mody I, Silva A. 2008. Neurofibromin regulation of ERK signaling modulates GABA release and learning. *Cell*. 135(3):549–560.
- Denaxa M, Neves G, Rabinowitz A, Kemlo S, Liadis P, Burrone J, Pachnis V. 2018. Modulation of apoptosis controls inhibitory interneuron number in the cortex. *Cell Rep*. 22(7):1710–1721.
- Digilio MC, Lepri F, Baban A, Dentici ML, Versacci P, Capolino R, Ferese R, De Luca A, Tartaglia M, Marino B et al. 2011. Rasopathies: clinical diagnosis in the first year of life. *Mol Syndromol*. 1(6):282–289.
- Doughty AH, Richards JB. 2002. Effects of reinforcer magnitude on responding under differential-reinforcement-of-low-rate schedules of rats and pigeons. *J Exp Anal Behav*. 78(1):17–30.
- Ehrman L, Nardini D, Ehrman S, Rizvi T, Gulick J, Krenz M, Dasgupta B, Robbins J, Ratner N, Nakafuku M et al. 2014. The protein tyrosine phosphatase SHP2 is required for the generation of oligodendrocyte progenitor cells and myelination in the mouse telencephalon. *J Neurosci*. 34(10):3767–3778.
- Fazzari P, Paternain AV, Valiente M, Pla R, Luján R, Lloyd K, Lerma J, Marín O, Rico B. 2010. Control of cortical GABA circuitry development by Nrg1 and Erbb4 signalling. *Nature*. 464(7293):1376–1380.
- Flames N, Long J, Garratt A, Fischer T, Gassmann M, Birchmeier C, Lai C, Rubenstein J, Marin O. 2004. Short- and long-range attraction of cortical GABAergic interneurons by neuregulin-1. *Neuron*. 44(2):251–261.
- Fowke TM, Galinsky R, Davidson JO, Wassink G, Karunasinghe RN, Prasad JD, Bennet L, Gunn AJ, Dean JM. 2018. Loss of interneurons and disruption of perineuronal nets in the cerebral cortex following hypoxia-ischaemia in near-term fetal sheep. *Sci Rep*. 8(1):17686.
- Fu Y, Tucciarone JM, Espinosa JS, Sheng N, Darcy DP, Nicoll RA, Huang ZJ, Stryker MP. 2014. A cortical circuit for gain control by behavioral state. *Cell*. 156(6):1139–1152.
- Gabay Y, Shahbari-Khateb E, Mendelsohn A. 2018. Feedback timing modulates probabilistic learning in adults with ADHD. *Sci Rep*. 8(1):15524.
- Galtrey CM, Fawcett JW. 2007. The role of chondroitin sulfate proteoglycans in regeneration and plasticity in the central nervous system. *Brain Res Rev*. 54(1):1–18.
- Garg S, Lehtonen A, Huson SM, Emsley R, Trump D, Evans DG, Green J. 2013. Autism and other psychiatric comorbidity in neurofibromatosis type 1: evidence from a population-based study. *Dev Med Child Neurol*. 55(2):139–145.
- Gauthier A, Furstoss O, Araki T, Chan R, Neel B, Kaplan D, Miller F. 2007. Control of CNS cell-fate decisions by Shp-2 and its dysregulation in Noonan syndrome. *Neuron*. 54(2):245–262.
- Gelman DM, Marín O. 2010. Generation of interneuron diversity in the mouse cerebral cortex. *Eur J Neurosci*. 31(12):2136–2141.
- Goldberg E, Jeong H, Kruglikov I, Tremblay R, Lazarenko R, Rudy B. 2011. Rapid developmental maturation of neocortical FS cell intrinsic excitability. *Cereb Cortex*. 21(3):666–682.
- Green T, Naylor PE, Davies W. 2017. Attention deficit hyperactivity disorder (ADHD) in phenotypically similar neurogenetic conditions: Turner syndrome and the Rasopathies. *J Neurodev Disord*. 9:25.
- Hensch T. 2005a. Critical period mechanisms in developing visual cortex. *Curr Top Dev Biol*. 69:215–+.
- Hensch TK. 2005b. Critical period plasticity in local cortical circuits. *Nat Rev Neurosci*. 6(11):877–888.
- Hill JC, Herbst K, Sanabria F. 2012. Characterizing operant hyperactivity in the spontaneously hypertensive rat. *Behav Brain Funct*. 8:5.
- Holter MC, Hewitt LT, Koebele SV, Judd JM, Xing L, Bimonte-Nelson HA, Conrad CD, Araki T, Neel BG, Snider WD et al. 2019. The Noonan syndrome-linked Raf1-L613V mutation drives increased glial number in the mouse cortex and enhanced learning. *PLoS Genet*. 15(4):e1008108.
- Hrvatín S, Hochbaum DR, Nagy MA, Cicconet M, Robertson K, Cheadle L, Zilionis R, Ratner A, Borges-Monroy R, Klein AM et al. 2018. Single-cell analysis of experience-dependent transcriptomic states in the mouse visual cortex. *Nat Neurosci*. 21(1):120–129.
- Hutton SR, Otis JM, Kim EM, Lamsal Y, Stuber GD, Snider WD. 2017. ERK/MAPK signaling is required for pathway-specific striatal motor functions. *J Neurosci*. 37(34):8102–8115.
- Inan M, Zhao M, Manuszak M, Karakaya C, Rajadhyaksha AM, Pickel VM, Schwartz TH, Goldstein PA, Manfredi G. 2016. Energy deficit in parvalbumin neurons leads to circuit dysfunction, impaired sensory gating and social disability. *Neurobiol Dis*. 93:35–46.
- Ishii A, Furusho M, Bansal R. 2013. Sustained activation of Erk1/2 Mapk in oligodendrocytes and Schwann cells enhances myelin growth and stimulates oligodendrocyte progenitor expansion. *J Neurosci*. 33(1):175–186.
- Johnson EM, Ishak AD, Naylor PE, Stevenson DA, Reiss AL, Green T. 2019. Ptpn11 gain-of-function mutations affect the developing human brain, memory, and attention. *Cereb Cortex*. 29(7):2915–2923.

- Kelsom C, Lu W. 2013. Development and specification of gabaergic cortical interneurons. *Cell Biosci.* 3(1):19.
- Kessarar N, Magno L, Rubin AN, Oliveira MG. 2014. Genetic programs controlling cortical interneuron fate. *Curr Opin Neurobiol.* 26:79–87.
- Klesse LJ, Meyers KA, Marshall CJ, Parada LF. 1999. Nerve growth factor induces survival and differentiation through two distinct signaling cascades in PC12 cells. *Oncogene.* 18(12):2055–2068.
- Kozorovitskiy Y, Saunders A, Johnson CA, Lowell BB, Sabatini BL. 2012. Recurrent network activity drives striatal synaptogenesis. *Nature.* 485(7400):646–650.
- Krencik R, Hokanson KC, Narayan AR, Dvornik J, Rooney GE, Rauen KA, Weiss LA, Rowitch DH, Ullian EM. 2015. Dysregulation of astrocyte extracellular signaling in Costello syndrome. *Sci Transl Med.* 7(286):286ra266.
- Krenz M, Gulick J, Osinska HE, Colbert MC, Molkentin JD, Robbins J. 2008. Role of ERK1/2 signaling in congenital valve malformations in Noonan syndrome. *Proc Natl Acad Sci U S A.* 105(48):18930–18935.
- Krishnan K, Wang BS, Lu J, Wang L, Maffei A, Cang J, Huang ZJ. 2015. Mecp2 regulates the timing of critical period plasticity that shapes functional connectivity in primary visual cortex. *Proc Natl Acad Sci U S A.* 112(34):E4782–E4791.
- Krueger DD, Osterweil EK, Chen SP, Tye LD, Bear MF. 2011. Cognitive dysfunction and prefrontal synaptic abnormalities in a mouse model of fragile x syndrome. *Proc Natl Acad Sci U S A.* 108(6):2587–2592.
- Kumar RA, Kara Mohamed S, Sudi J, Conrad DF, Brune C, Badner JA, Gilliam TC, Nowak NJ, Cook EH, Dobyns WB et al. 2008. Recurrent 16p11.2 microdeletions in autism. *Hum Mol Genet.* 17(4):628–638.
- Lajiness JD, Snider P, Wang J, Feng GS, Krenz M, Conway SJ. 2014. Shp-2 deletion in postmigratory neural crest cells results in impaired cardiac sympathetic innervation. *Proc Natl Acad Sci U S A.* 111(14):E1374–E1382.
- Lavdas AA, Grigoriou M, Pachnis V, Parnavelas JG. 1999. The medial ganglionic eminence gives rise to a population of early neurons in the developing cerebral cortex. *J Neurosci.* 19(18):7881–7888.
- Li X, Newbern J, Wu Y, Morgan-Smith M, Zhong J, Charron J, Snider W. 2012. Mek is a key regulator of gliogenesis in the developing brain. *Neuron.* 75(6):1035–1050.
- Lim L, Mi D, Llorca A, Marín O. 2018. Development and functional diversification of cortical interneurons. *Neuron.* 100(2):294–313.
- Madisen L, Zwingman TA, Sunkin SM, Oh SW, Zariwala HA, Gu H, Ng LL, Palmiter RD, Hawrylycz MJ, Jones AR et al. 2010. A robust and high-throughput cre reporting and characterization system for the whole mouse brain. *Nat Neurosci.* 13(1):133–140.
- Malik R, Pai EL, Rubin AN, Stafford AM, Angara K, Minasi P, Rubenstein JL, Sohal VS, Vogt D. 2019. Tsc1 represses parvalbumin expression and fast-spiking properties in somatostatin lineage cortical interneurons. *Nat Commun.* 10(1):4994.
- Mardinly AR, Spiegel I, Patrizi A, Centofante E, Bazinet JE, Tzeng CP, Mandel-Brehm C, Harmin DA, Adesnik H, Fagiolini M et al. 2016. Sensory experience regulates cortical inhibition by inducing IGF1 in VIP neurons. *Nature.* 531(7594):371–375.
- Marín O, Rubenstein J. 2003. Cell migration in the forebrain. *Annu Rev Neurosci.* 26:441–483.
- Martin P, Pognonec P. 2010. Erk and cell death: cadmium toxicity, sustained erk activation and cell death. *FEBS J.* 277(1):39–46.
- Mayer C, Hafemeister C, Bandler RC, Machold R, Batista Brito R, Jaglin X, Allaway K, Butler A, Fishell G, Satija R. 2018. Developmental diversification of cortical inhibitory interneurons. *Nature.* 555(7697):457–462.
- Mi D, Li Z, Lim L, Li M, Moissidis M, Yang Y, Gao T, Hu TX, Pratt T, Price DJ et al. 2018. Early emergence of cortical interneuron diversity in the mouse embryo. *Science.* 360(6384):81–85.
- McCormick DA, Connors BW, Lighthall JW, Prince DA. 1985. Comparative electrophysiology of pyramidal and sparsely spiny stellate neurons of the neocortex. *J Neurophysiol.* 54(4):782–806.
- McRae PA, Porter BE. 2012. The perineuronal net component of the extracellular matrix in plasticity and epilepsy. *Neurochem Int.* 61(7):963–972.
- Miguel CS, Chaim-Avancini TM, Silva MA, Louzã MR. 2015. Neurofibromatosis type 1 and attention deficit hyperactivity disorder: a case study and literature review. *Neuropsychiatr Dis Treat.* 11:815–821.
- Miyoshi G, Hjerling-Leffler J, Karayannis T, Sousa V, Butt S, Battiste J, Johnson J, Machold R, Fishell G. 2010. Genetic fate mapping reveals that the caudal ganglionic eminence produces a large and diverse population of superficial cortical interneurons. *J Neurosci.* 30(5):1582–1594.
- Monory K, Massa F, Egertová M, Eder M, Blaudzun H, Westbroek R, Kelsch W, Jacob W, Marsch R, Ekker M et al. 2006. The endocannabinoid system controls key epileptogenic circuits in the hippocampus. *Neuron.* 51(4):455–466.
- Morishita H, Cabungcal J, Chen Y, Do K, Hensch T. 2015. Prolonged period of cortical plasticity upon redox dysregulation in fast-spiking interneurons. *Biol Psychiatry.* 78(6):396–402.
- Nateri AS, Raivich G, Gebhardt C, Da Costa C, Naumann H, Vreugdenhil M, Makwana M, Brandner S, Adams RH, Jefferys JG et al. 2007. ERK activation causes epilepsy by stimulating NMDA receptor activity. *EMBO J.* 26(23):4891–4901.
- Nichols J, Bjorklund GR, Newbern J, Anderson T. 2018. Parvalbumin fast-spiking interneurons are selectively altered by paediatric traumatic brain injury. *J Physiol.* 596(7):1277–1293.
- Okaty B, Miller M, Sugino K, Hempel C, Nelson S. 2009. Transcriptional and electrophysiological maturation of neocortical fast-spiking gabaergic interneurons. *J Neurosci.* 29(21):7040–7052.
- Osterweil EK, Krueger DD, Reinhold K, Bear MF. 2010. Hypersensitivity to mGluR5 and Erk1/2 leads to excessive protein synthesis in the hippocampus of a mouse model of fragile x syndrome. *J Neurosci.* 30, 46:15616–15627.
- Ozkan ED, Creson TK, Kramár EA, Rojas C, Seese RR, Babayan AH, Shi Y, Lucero R, Xu X, Noebels JL et al. 2014. Reduced cognition in Syngap1 mutants is caused by isolated damage within developing forebrain excitatory neurons. *Neuron.* 82(6):1317–1333.
- Paluszkiwicz SM, Martin BS, Huntsman MM. 2011. Fragile x syndrome: the GABAergic system and circuit dysfunction. *Dev Neurosci.* 33(5):349–364.
- Paul A, Crow M, Raudales R, He M, Gillis J, Huang ZJ. 2017. Transcriptional architecture of synaptic communication delineates GABAergic neuron identity. *Cell.* 171(3):522, e520–539.
- Perrinjaquet M, Sjostrand D, Moliner A, Zechel S, Lamballe F, Maina F, Ibanez C. 2011. Met signaling in GABAergic neuronal precursors of the medial ganglionic eminence restricts

- GDNF activity in cells that express Gfr alpha 1 and a new transmembrane receptor partner. *J Cell Sci.* 124(16):2797–2805.
- Pham TA, Graham SJ, Suzuki S, Barco A, Kandel ER, Gordon B, Lickey ME. 2004. A semi-persistent adult ocular dominance plasticity in visual cortex is stabilized by activated CREB. *Learn Mem.* 11(6):738–747.
- Pierpont E, Hudock R, Foy A, Semrud-Clikeman M, Pierpont M, Berry S, Shanley R, Rubin N, Sommer K, Moertel C. 2018. Social skills in children with rasopathies: a comparison of Noonan syndrome and neurofibromatosis type 1. *J Neurodev Disord.* 10.
- Pizzorusso T, Medini P, Berardi N, Chierzi S, Fawcett JW, Maffei L. 2002. Reactivation of ocular dominance plasticity in the adult visual cortex. *Science.* 298(5596):1248–1251.
- Pozas E, Ibanez C. 2005. Gdnf and gfr alpha 1 promote differentiation and tangential migration of cortical gabaergic neurons. *Neuron.* 45(5):701–713.
- Pucilowska J, Vithayathil J, Pagani M, Kelly C, Karlo JC, Robol C, Morella I, Gozzi A, Brambilla R, Landreth GE. 2018. Pharmacological inhibition of Erk signaling rescues pathophysiology and behavioral phenotype associated with 16p11.2 chromosomal deletion in mice. *J Neurosci.* 38(30):6640–6652.
- Rauen K, Chakravarti A, Green E. 2013. The rasopathies. *Annu Rev Genomics Hum Genet.* 14:355–369.
- Rojas-Leguizamón M, Baroja JL, Sanabria F, Orduña V. 2018. Response-inhibition capacity in spontaneously hypertensive and Wistar rats: acquisition of fixed minimum interval performance and responsiveness to d-amphetamine. *Behav Pharmacol.* 29(8):668–675.
- Roskoski R. 2012. Erk1/2 map kinases: structure, function, and regulation. *Pharmacol Res.* 66(2):105–143.
- Rudy B, Mcbain C. 2001. Kv3 channels: voltage-gated K⁺ channels designed for high-frequency repetitive firing. *Trends Neurosci.* 24, 9:517–526.
- Rudy B, Fishell G, Lee S, Hjerling-Leffler J. 2011. Three groups of interneurons account for nearly 100% of neocortical gabaergic neurons. *Dev Neurobiol.* 71(1):45–61.
- Samuels I, Saitta S, Landreth G. 2009. Map'ing CNS development and cognition: an ERKsome process. *Neuron.* 61(2):160–167.
- Seidman LJ, Valera EM, Makris N, Monuteaux MC, Boriell DL, Kelkar K, Kennedy DN, Caviness VS, Bush G, Aleari M et al. 2006. Dorsolateral prefrontal and anterior cingulate cortex volumetric abnormalities in adults with attention-deficit/hyperactivity disorder identified by magnetic resonance imaging. *Biol Psychiatry.* 60(10):1071–1080.
- Sorg BA, Berretta S, Blacktop JM, Fawcett JW, Kitagawa H, Kwok JC, Miquel M. 2016. Casting a wide net: role of perineuronal nets in neural plasticity. *J Neurosci.* 36(45):11459–11468.
- Stanco A, Pla R, Vogt D, Chen Y, Mandal S, Walker J, Hunt R, Lindtner S, Erdman C, Pieper A et al. 2014. Npas1 represses the generation of specific subtypes of cortical interneurons. *Neuron.* 84(5):940–953.
- Steuillet P, Cabungcal JH, Coyle J, Didriksen M, Gill K, Grace AA, Hensch TK, AS LM, Lindemann L, Maynard TM et al. 2017. Oxidative stress-driven parvalbumin interneuron impairment as a common mechanism in models of schizophrenia. *Mol Psychiatry.* 22(7):936–943.
- Steward O, Torre E, Tomasulo R, Lothman E. 1992. Seizures and the regulation of astroglial gene-expression. *Epilepsy Res.* 7:197–209.
- Stringer J. 1996. Repeated seizures increase GFAP and vimentin in the hippocampus. *Brain Res.* 717(1–2):147–153.
- Suzuki S, Al-Noori S, Butt SA, Pham TA. 2004. Regulation of the Creb signaling cascade in the visual cortex by visual experience and neuronal activity. *J Comp Neurol.* 479(1):70–83.
- Tamamaki N, Fujimori KE, Takauji R. 1997. Origin and route of tangentially migrating neurons in the developing neocortical intermediate zone. *J Neurosci.* 17(21):8313–8323.
- Tewari BP, Chaunsali L, Campbell SL, Patel DC, Goode AE, Sontheimer H. 2018. Perineuronal nets decrease membrane capacitance of peritumoral fast spiking interneurons in a model of epilepsy. *Nat Commun.* 9(1):4724.
- Tidyman W, Rauen K. 2016. Pathogenetics of the Rasopathies. *Hum Mol Genet.* 25(R2):R123–R132.
- Tyssowski KM, NR DS, Cho JH, Dunn CJ, Poston RG, Carty CE, Jones RD, Chang SM, Romeo P, Wurzelmann MK et al. 2018. Different neuronal activity patterns induce different gene expression programs. *Neuron.* 98(3):530, e511–546.
- Vogt D, KKA C, Lee AT, Sohal VS, JLR R. 2015. The parvalbumin/somatostatin ratio is increased in Pten mutant mice and by human Pten ASD alleles. *Cell Rep.* 11(6):944–956.
- Vong L, Ye C, Yang Z, Choi B, Chua S, Lowell BB. 2011. Leptin action on GABAergic neurons prevents obesity and reduces inhibitory tone to POMC neurons. *Neuron.* 71(1):142–154.
- Vorstman JA, Staal WG, van Daalen E, van Engeland H, Hochstenbach PF, Franke L. 2006. Identification of novel autism candidate regions through analysis of reported cytogenetic abnormalities associated with autism. *Mol Psychiatry.* 11(1) 1:18–28.
- Walsh KS, Vélez JI, Kardel PG, Imas DM, Muenke M, Packer RJ, Castellanos FX, Acosta MT. 2013. Symptomatology of autism spectrum disorder in a population with neurofibromatosis type 1. *Dev Med Child Neurol.* 55(2):131–138.
- Watterson E, Mazur GJ, Sanabria F. 2015. Validation of a method to assess adhd-related impulsivity in animal models. *J Neurosci Methods.* 252:36–47.
- Wei Y, Han X, Zhao C. 2020. Pdk1 regulates the survival of the developing cortical interneurons. *Mol Brain.* 13(1):65.
- Wonders C, Anderson S. 2006. The origin and specification of cortical interneurons. *Nat Rev Neurosci.* 7(9):687–696.
- Xing L, Larsen R, Bjorklund G, Li X, Wu Y, Philpot BD, Snider W, Newbern J. 2016. Layer specific and general requirements for Erk/Mapk signaling in the developing neocortex. *Elife.* 5.
- Xu Q, Tam M, Anderson SA. 2008. Fate mapping Nkx2.1-lineage cells in the mouse telencephalon. *J Comp Neurol.* 506(1):16–29.
- Yoon G, Rosenberg J, Blaser S, Rauen K. 2007. Neurological complications of cardio-facio-cutaneous syndrome. *Dev Med Child Neurol.* 49(12):894–899.